Journal of Medicinal Chemistry

pubs.acs.org/jmc Article

The Discovery of Novel ACA Derivatives as Specific TRPM2 Inhibitors that Reduce Ischemic Injury Both In Vitro and In Vivo

Han Zhang,[#] Peilin Yu,[#] Hongwei Lin, Zefang Jin, Siqi Zhao, Yi Zhang, Qingxia Xu, Hongwei Jin, Zhenming Liu, Wei Yang,* and Liangren Zhang*

Cite This: J. Med. Chem. 2021, 64, 3976−3996 Read Online

ACCESS | Metrics & More | Article Recommendations | Supporting Information

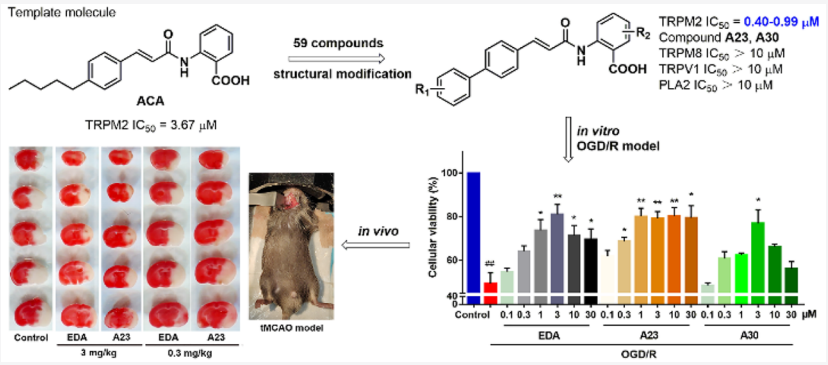

ABSTRACT: The transient receptor potential melastatin 2 (TRPM2) channel is associated with ischemia/reperfusion injury, inflammation, cancer, and neurodegenerative diseases. However, the limit of specific inhibitors impedes the development of TRPM2-targeted therapeutic agents. To discover more potent and selective TRPM2 inhibitors, 59 *N*-(*p*-amylcinnamoyl) anthranilic acid (ACA) derivatives were synthesized and evaluated using calcium imaging and electrophysiology approaches. Systematic structure−activity relationship studies resulted in some potent compounds inhibiting the TRPM2 channel with sub-micromolar half-maximal inhibitory concentration values. Among them, the preferred compound **A23** exhibited TRPM2 selectivity over TRPM8 and TRPV1 channels as well as phospholipase A2 and showed neuroprotective activity in vitro. Following pharmacokinetic studies, **A23** was further evaluated in a transient middle cerebral artery occlusion model in vivo, which significantly reduced cerebral infarction. These data indicate that **A23** might serve as a useful tool for TRPM2-related research as well as a lead compound for the development of therapeutic agents for ischemic injury.

INTRODUCTION

The transient receptor potential (TRP) channel family is one of the largest cation channel families, which exhibits a large variety of functional properties and plays diverse cellular and physiological roles.[1,2] In mammals, 28 different TRP proteins have been identified, which are often grouped into six TRP subfamilies: canonical (TRPC), vanilloid (TRPV), melastatin (TRPM), ankyrin (TRPA), polycystin (TRPP), and mucolipin (TRPML), according to amino acid sequence relatedness.[3] The TRPM subfamily comprises eight subtypes, which can be divided into four pairs based on their amino acid sequence homology: TRPM1/TRPM3, TRPM2/TRPM8, TRPM4/TRPM5, and TRPM6/TRPM7.[4]

The TRPM2 channel, first isolated from the human brain in 1998, is a cation channel permeable for calcium (Ca^{2+}).[5] It exhibits widespread distribution in a number of tissues and cells, with the highest expression in the brain and a relatively high expression in bone marrow cells and macrophages.[6] Given its role in Ca^{2+} mobilization as a crucial endogenous sensor of reactive oxygen species (ROS), the TRPM2 channel participates in many calcium-dependent physiological and pathophysiological processes, such as pro-inflammatory cytokine production in immune cells, endothelial permeability, insulin release by pancreatic *β*-cells, warmth sensation, and cell death.[7,8] Cell death is the most outstanding and common consequence of TRPM2 channel activation, and its excessive activation can lead to cytotoxicity due to Ca^{2+} overload, which is involved in ischemia/reperfusion (I/R)-induced damage, Alzheimer's disease, Parkinson's disease, amyotrophic lateral sclerosis, neurovascular dysfunction, cardiovascular disorders, diabetes, chronic kidney disease, liver injury, cancer, and inflammatory diseases.[9−13]

Received: December 10, 2020
Published: March 30, 2021

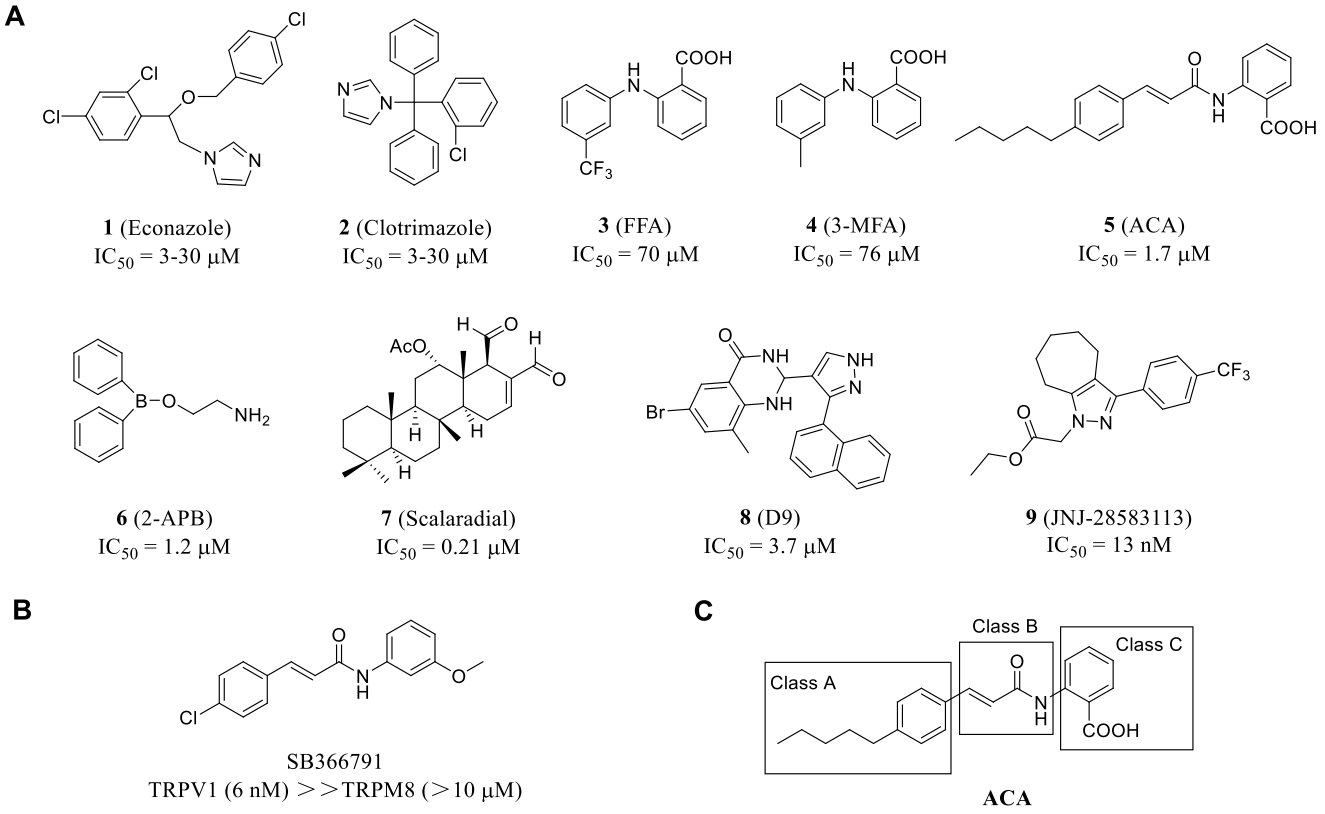

Figure 1. Chemical structures of representative inhibitors. (A) Chemical structures and inhibitory activities of representative TRPM2 inhibitors. (B) Chemical structures and inhibitory activities of SB366791. (C) Design of ACA derivatives as TRPM2 inhibitors. ACA was divided into pentyl aromatic ring moiety (Class A), linker moiety (Class B), and carboxyl aromatic ring moiety (Class C).

Ischemic stroke is the second leading cause of death after ischemic heart disease and accounts for 9% of deaths worldwide.[14] Intravenous thrombolysis and endovascular intervention are clinically applicable treatments for stroke, but both have a narrow therapeutic window and might cause a reperfusion injury. Therefore, current measures to protect the brain against stroke damage are insufficient.[15,16] ROS have been implicated in brain injury after an ischemic stroke and can damage cellular macromolecules leading to autophagy, apoptosis, and necrosis. Moreover, the restoration of blood flow leads to a reperfusion injury that can largely be attributed to a second burst of ROS generation, which is an important cellular mechanism for the progressive decline in cognitive function and I/R-induced brain damage.[17] The TRPM2 channel has been extensively scrutinized for its role in mediating delayed neuronal cell death. A number of studies using various in vitro and in vivo I/R models have gathered substantial evidence to support a critical role for the TRPM2 channel in mediating neuronal cell death due to reperfusion, leading to I/R-induced brain damage.[12,18−20] Even though there is evidence that TRPM2 appears to be a viable target for therapeutic interventions for ischemic stroke, preclinical studies have been limited by the lack of TRP-subtype specific and potent inhibitors. Therefore, the development of specific TRPM2 inhibitors has garnered increasing attention for both academic functional studies and clinical applications.

The chemical structures and inhibitory activities of representative TRPM2 inhibitors are summarized in Figure 1A. Several initially discovered TRPM2 inhibitors have inhibitory activities at micromolar levels, including econazole (**1**), clotrimazole (**2**), flufenamic acid (**3**, FFA), 2-(3-methylphenyl) aminobenzoic acid (**4**, 3-MFA), *N*-(*p*-amylcinnamoyl) anthranilic acid (**5**, ACA), and 2-aminoethoxydiphenyl borate (**6**, 2-APB).[21−25] However, most of these compounds lack specificity, especially considering that the TRPM8 channel has a high homology with TRPM2.[26] Marine-derived scalaradial (**7**) was identified as a TRPM2 inhibitor, but it has indirect effects on the channel.[27] We recently discovered 2,3-dihydroquinazolin-4(1*H*)-one derivative **D9** (**8**), which showed a half-maximal inhibitory concentration (IC_{50}) value of 3.7 μM against TRPM2 and did not affect the TRPM8 channel.[28] In addition, two more potent TRPM2 inhibitors were recently identified. JNJ-28583113 (**9**) is the most potent TRPM2 inhibitor in vitro, but it has stability difficulties in vivo.[29] tatM2NX is a cell-permeable peptide inhibitor of TRPM2, which exhibits neuroprotective effects in vivo, but its druggability needs further evaluation.[30] Several endogenous ligand analogues are thought to selectively inhibit TRPM2, but poor membrane permeability and stability limit their application.[31,32] Currently, the number of reported TRPM2 inhibitors is limited; hence, there is an urgent need to develop novel small-molecule TRPM2 inhibitors with improvements in both potency and selectivity, which will not only provide molecular tools for better understanding of the channel functions in cell biology but will also lead to potential clinical therapeutic agents for ischemic injury and other related diseases.

ACA is a well-described inhibitor that is widely used in studies on TRPM2. The administration of ACA decreases hippocampal cell death and infarct size in ischemic stroke, improves insulin sensitivity in adipose tissue during Angiotensin II-induced hypertension, and attenuates the neuro-

https://doi.org/10.1021/acs.jmedchem.0c02129
J. Med. Chem. 2021, 64, 3976−3996

Scheme 1. Synthesis of Compounds A1−A33[a]

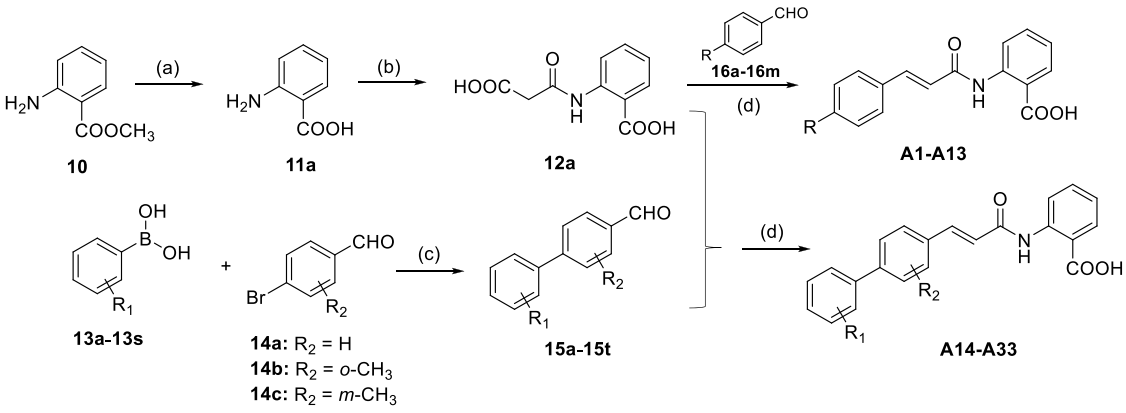

16a, A1: R = H
16b, A2: R = Cl
16c, A3: R = methyl
16d, A4: R = ethyl
16e, A5: R = *n*-propyl
16f, A6: R = isopropyl
16g, A7: R = tertiary butyl
16h, A8: R = ethoxyl
16i, A9: R = isopropylcarbamoyl
16j, A10: R = pyridin-3-yl
16k, A11: R = piperidin-1-yl
16l, A12: R = morpholinyl
16m, A13: R = phenyl
13a, 15a, A14: R_1 = H, R_2 = *o*-methyl
13a, 15b, A15: R_1 = H, R_2 = *m*-methyl
13b, 15c, A16: R_1 = *o*-methyl
13c, 15d, A17: R_1 = *o*-methoxyl
13d, 15e, A18: R_1 = *o*-fluorine
13e, 15f, A19: R_1 = *o*-trifluoromethyl
13f, 15g, A20: R_1 = *m*-methyl
13g, 15h, A21: R_1 = *m*-methoxyl
13h, 15i, A22: R_1 = *m*-fluorine
13i, 15j, A23: R_1 = *m*-trifluoromethyl
13j, 15k, A24: R_1 = *p*-methyl
13k, 15l, A25: R_1 = *p*-methoxyl
13l, 15m, A26: R_1 = *p*-fluorine
13m, 15n, A27: R_1 = *p*-trifluoromethyl
13n, 15o, A28: R_1 = *m*-chlorine
13o, 15p, A29: R_1 = *m*-bromine
13p, 15q, A30: R_1 = *m*-nitro
13q, 15r, A31: R_1 = *p*-ethyl
13r, 15s, A32: R_1 = *p*-isopropyl
13s, 15t, A33: R_1 = *p*-tertiary butyl

[a]Reagents and conditions: (a) NaOH, THF, ethanol, H_2O, reflux, 4 h; (b) 2,2-dimethyl-1,3-dioxane-4,6-dione, toluene, reflux, 3 h; (c) $Pd(PPh_3)_4$, K_2CO_3, dioxane, H_2O, 105 °C, 24 h, (d) piperidine, toluene, reflux, 3 h, then rt, 1 h.

inflammation of okadaic acid-induced neurodegeneration.[9,33−36] However, the inhibitory effect of ACA on the TRPM2 channel is nonspecific. It is often used as a broad-spectrum inhibitor for the characterization of phospholipase A2 (PLA2)-mediated pathways in early studies and also blocks other TRP channels (TRPM8, TRPC3, TRPC6, and TRPV1).[24,37,38] The inhibitory effect of ACA on the TRP channel is in the following order: TRPM2, TRPM8 > TRPC6 > TRPV1. A side-by-side comparison of ACA with the TRPV1 selective antagonist SB366791 (Figure 1B) showed that *N*-phenylcinnamamide forms the core for a class of TRP channel inhibitors.[39] Therefore, the specificity of the *N*-phenylcinnamamide structures to a particular TRP channel might be achieved through a specific set of substituents.

In this study, we report a successful case of modification of the known TRPM2 inhibitor ACA, which led to the discovery of novel potent and selective inhibitors of the TRPM2 channel. Among the 59 synthesized compounds, the promising compound **A23** inhibited the TRPM2 channel with a submicromolar IC_{50} value and displayed selectivity against the TRPM8 and TRPV1 channels as well as PLA2. Further pharmacological and pharmacokinetic (PK) experiments revealed that **A23** had marked neuroprotective effects against oxygen glucose deprivation/reperfusion (OGD/R)-induced cell death in vitro and transient middle cerebral artery occlusion (tMCAO)-induced ischemic stroke in vivo and exhibited a high plasma exposure. Beyond facilitating the discovery of novel specific TRPM2 inhibitors, the finding of this study will provide a new tool for studying the TRPM2 molecular mechanisms in cell physiology and pathophysiology and might promote therapeutic advances for ischemic injury and other related diseases.

RESULTS AND DISCUSSION

Chemistry. Structural optimization was performed on ACA to discover more active inhibitors of the TRPM2 channel. As shown in Figure 1C, we divided ACA briefly into the pentyl aromatic ring moiety (Class A), linker moiety (Class B), and carboxyl aromatic ring moiety (Class C). The structure of each moiety was modified separately to investigate the influence of different structural fragments on the inhibitory activity against the TRPM2 channel, to obtain a thorough understanding of the structure−activity relationship (SAR). The general synthetic routes for preparation of Classes A, B, and C are described in Schemes 1−8.

Scheme 2. Synthesis of Compound B1[a]

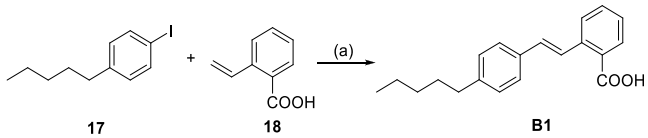

[a]Reagents and conditions: (a) $Pd(OAc)_2$, Et_3N, CH_3CN, reflux, 12 h.

Scheme 3. Synthesis of Compound B2[a]

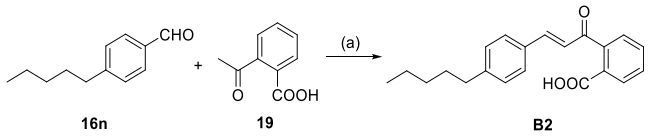

[a]Reagents and conditions: (a) NaOH, ethanol, rt, 20 min.

Methyl 2-aminobenzoate (**10**) was hydrolyzed with sodium hydroxide to give 2-aminobenzoic acid (**11a**), which then was reacted with 2,2-dimethyl-1,3-dioxane-4,6-dione in toluene to form carboxyacetamidobenzoic acid (**12a**). Biphenylcarbaldehyde derivatives (**15a−15t**) were synthesized by the Suzuki coupling reaction from substituted benzboric acids (**13a−13s**) and 4-bromobenzaldehyde derivatives (**14a−14c**). Compounds **A1−A33** were prepared from **12a** through the

https://doi.org/10.1021/acs.jmedchem.0c02129
J. Med. Chem. 2021, 64, 3976−3996

Scheme 4. Synthesis of Compound B3[a]

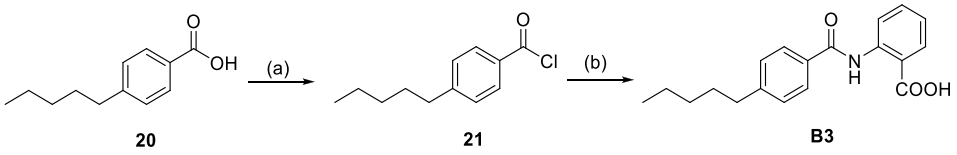

[a]Reagents and conditions: (a) $SOCl_2$, reflux, 4 h; (b) **11a**, Et_3N, THF, 0 °C, 15 min, then 60 °C, 3 h.

Scheme 5. Synthesis of Compound B4[a]

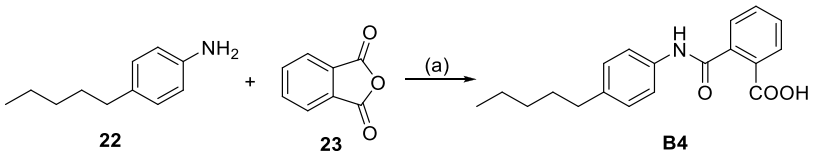

[a]Reagents and conditions: (a) acetone, rt, 2 h.

Scheme 6. Synthesis of Compounds C1−C17[a]

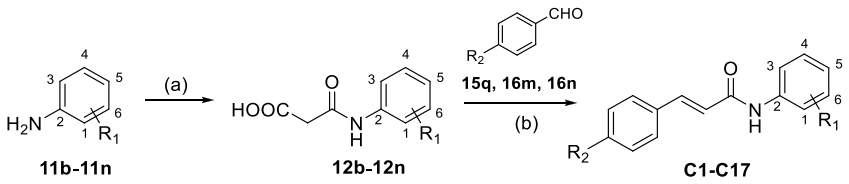

11b, 12b, C1: R_1 = 6-COOH; R_2 = *n*-pentyl
11c, 12c, C2: R_1 = 5-COOH; R_2 = *n*-pentyl
11d, 12d, C3: R_1 = 1-COOH-3-CH_3; R_2 = *n*-pentyl
11e, 12e, C4: R_1 = 1-COOH-3,4-CH_3; R_2 = *n*-pentyl
11f, 12f, C5: R_1 = 1-COOH-3-CH_3-5-Cl; R_2 = *n*-pentyl
11g, 12g, C6: R_1 = 1-COOH-3-Cl; R_2 = *n*-pentyl
11h, 12h, C7: R_1 = 1-COOH-4-CH_3; R_2 = *n*-pentyl
11h, 12h, C8: R_1 = 1-COOH-4-CH_3; R_2 = *m*-nitrophenyl
11i, 12i, C9: R_1 = 1-COOH-4,5-2F; R_2 = *n*-pentyl
11j, 12j, C10: R_1 = 1-COOH-4-Cl; R_2 = *n*-pentyl
11j, 12j, C11: R_1 = 1-COOH-4-Cl; R_2 = phenyl
11k, 12k, C12: R_1 = 1-COOH-5-CH_3; R_2 = *n*-pentyl
11l, 12l, C13: R_1 = 1-COOH-5-Br; R_2 = *n*-pentyl
11m, 12m, C14: R_1 = 1-COOH-5-F; R_2 = phenyl
11n, 12n, C15: R_1 = 1-COOH-5-Cl; R_2 = phenyl
11l, 12l, C16: R_1 = 1-COOH-5-Br; R_2 = phenyl
11l, 12l, C17: R_1 = 1-COOH-5-Br; R_2 = *m*-nitrophenyl

[a]Reagents and conditions: (a) 2,2-dimethyl-1,3-dioxane-4,6-dione, toluene, reflux, 3 h; (b) piperidine, toluene, reflux, 3 h, then rt, 1 h.

Scheme 7. Synthesis of Compound C18[a]

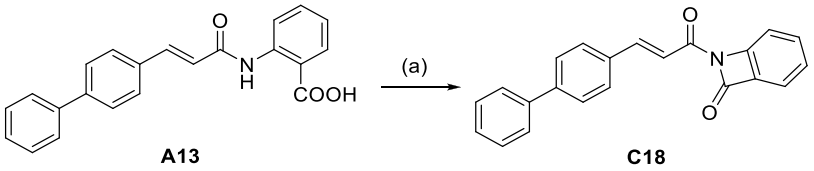

[a]Reagents and conditions: (a) acetic anhydride, reflux, 2 h.

Knoevenagel reaction with commercially available benzaldehyde derivatives (**16a−16m**) or synthesized biphenylcarbaldehydes **15a−15t** by the catalysis of piperidine (Scheme 1).[28,40]

Coupling of the 1-iodo-4-pentylbenzene (**17**) with 2-vinylbenzoic acid (**18**) under the Heck conditions produced compound **B1** (Scheme 2).[41]

Compound **B2** was prepared through an aldol condensation between 4-pentylbenzaldehyde (**16n**) and 2-acetylbenzoic acid (**19**) in ethanol (Scheme 3).[42]

Treatment of 4-pentylbenzoic acid (**20**) with thionyl chloride yielded 4-pentylbenzoyl chloride (**21**), which then was reacted with **11a** in the presence of catalytic amounts of triethylamine to form compound **B3** (Scheme 4).

4-Pentylaniline (**22**) was reacted with isobenzofuran-1,3-dione (**23**) in acetone to afford compound **B4** (Scheme 5).[43]

As aforementioned, aminobenzoic acid derivatives (**11b−11n**) were reacted with 2,2-dimethyl-1,3-dioxane-4,6-dione to produce carboxyacetamidobenzoic acid derivatives (**12b−12n**). Subsequently, piperidine-catalyzed Knoevenagel reactions of **12b−12n** and benzaldehyde derivatives (**15q**, **16m**, or **16n**) provided compounds **C1−C17** (Scheme 6).[40]

A dehydration reaction was accomplished by combining compound **A13** with acetic anhydride to form compound **C18** (Scheme 7).

Knoevenagel reactions of benzaldehyde derivatives (**16m** or **16n**) and malonic acid produced cinnamic acids (**24a**, **24b**), which then were reacted with thionyl chloride to yield cinnamoyl chlorides (**25a**, **25b**). Compounds **C19−C22** were prepared from 2,3-dihydroquinolin-4(1*H*)-one or 1,2,3,4-tetrahydro-5*H*-benzo[*b*]azepin-5-one with compound **25a** or **25b** in the presence of triethylamine (Scheme 8).

https://doi.org/10.1021/acs.jmedchem.0c02129
J. Med. Chem. 2021, 64, 3976−3996

Scheme 8. Synthesis of Compounds C19−C22[a]

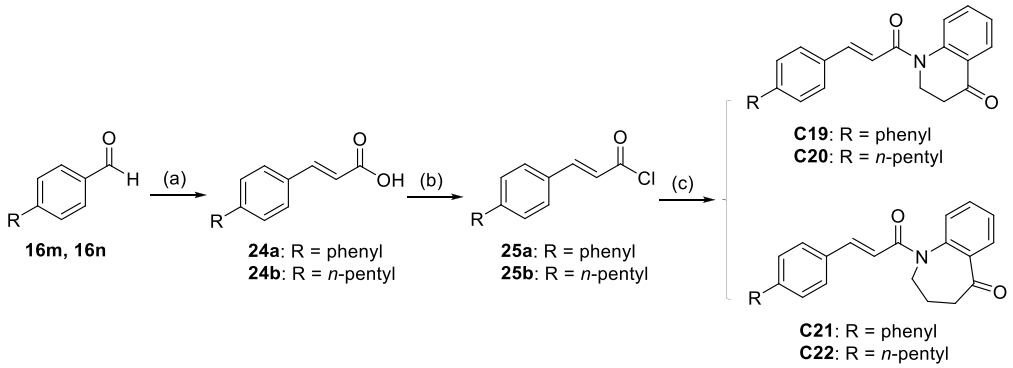

[a]Reagents and conditions: (a) malonic acid, piperidine, toluene, reflux, 3 h, then rt, 1 h; (b) $SOCl_2$, reflux, 4 h; (c) 2,3-dihydroquinolin-4(1*H*)-one or 1,2,3,4-tetrahydro-5*H*-benzo[*b*]azepin-5-one, Et_3N, THF, 0 °C, 15 min, then 60 °C, 3 h.

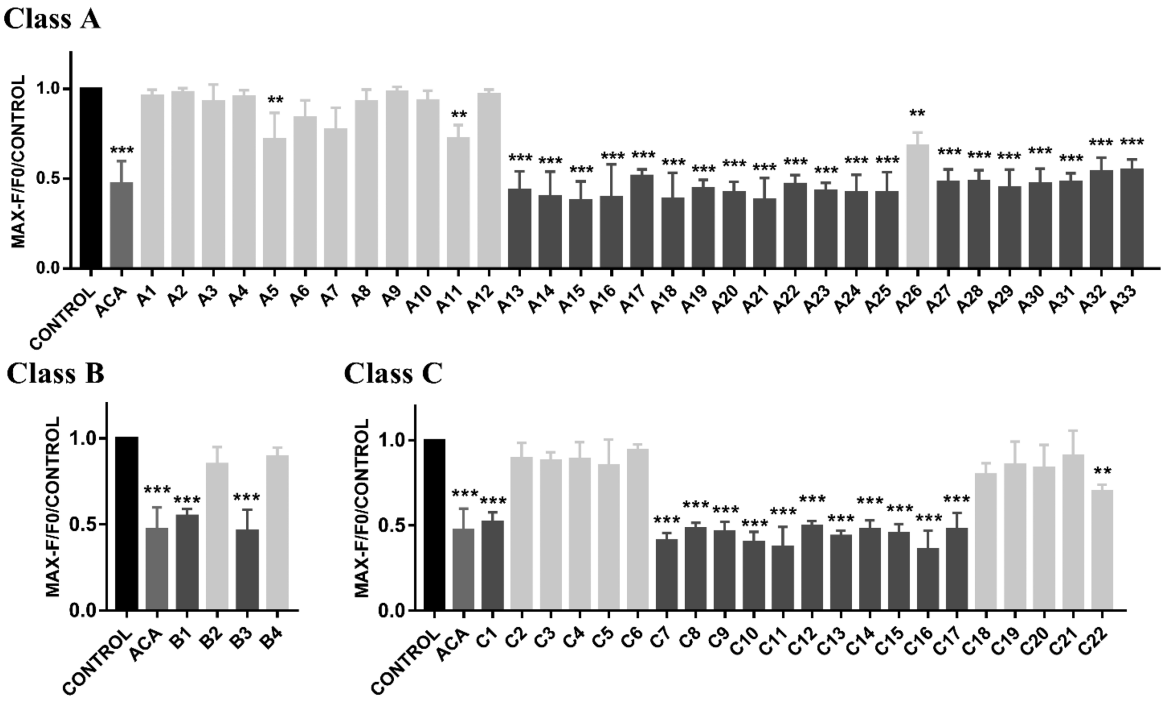

Figure 2. Inhibitory activity of 30 μM compounds **A1−A33**, **B1−B4**, and **C1−C22** against the TRPM2 channel preliminarily evaluated through a calcium imaging method. The concentration of agonist (H_2O_2) is 1 mM. Data are presented as the mean ± SD from at least three independent experiments ($n \geq 3$), and ***$P < 0.005$, **$P < 0.01$, *$P < 0.05$, test groups compared to the control group, one-way ANOVA, Dunnett's multiple comparison test.

Inhibitory Activity and SAR. A total of 59 compounds (Figure S1) were synthesized, and their biological activities were investigated. Fluorescent calcium imaging was used to preliminarily evaluate the inhibitory activity of these 59 compounds in human embryonic kidney (HEK) 293T cells stably overexpressing the human TRPM2 channel. As measured by intracellular Fluo 3 fluorescence, 38 compounds significantly suppressed hydrogen peroxide (H_2O_2)-induced Ca^{2+} influx after being incubated with cells for 30 min at a concentration of 30 μM (Figure 2). Among them, 34 compounds reduced the Ca^{2+} fluorescence increase by ~50% compared with vehicle-treated cells. Their inhibitory activity against the TRPM2 channel was confirmed in whole-cell patch-clamp experiments (Figure 3, Table S1). At the concentration of 1 μM, 22 compounds inhibited more than 45% of TRPM2 currents, which were further tested at 0.3 μM. The concentration-dependent response curves of compounds that blocked more than 45% of TRPM2 currents at the concentration of 0.3 μM were plotted to calculate IC_{50} values. Six compounds, that is, **A22**, **A23**, **A30**, **C7**, **C12**, and **C16**, gave IC_{50} values of 398−987 nM (Figure 4, Table S1). The TRPM2 nonspecific inhibitor ACA was used as a positive control with an IC_{50} value of 3.67 μM.

As shown in Figure 2, Figure 3, and Table S1, replacing the *n*-pentyl of ACA with hydrogen (**A1**), chlorine (**A2**), ethoxyl (**A8**), isopropylcarbamoyl (**A9**), and various alkyl chains (**A3−A7**) resulted in no or decreased inhibitory activity, showing that the inhibitory activity on the TRPM2 channel decreased with the shortening of the alkyl chain length. When the *n*-pentyl of ACA was replaced with six-member N-containing heterocyclic substitution groups, that is, pyridin-3-yl (**A10**), piperidin-1-yl (**A11**), and morpholinyl (**A12**), a lower potency

https://doi.org/10.1021/acs.jmedchem.0c02129
J. Med. Chem. 2021, 64, 3976−3996

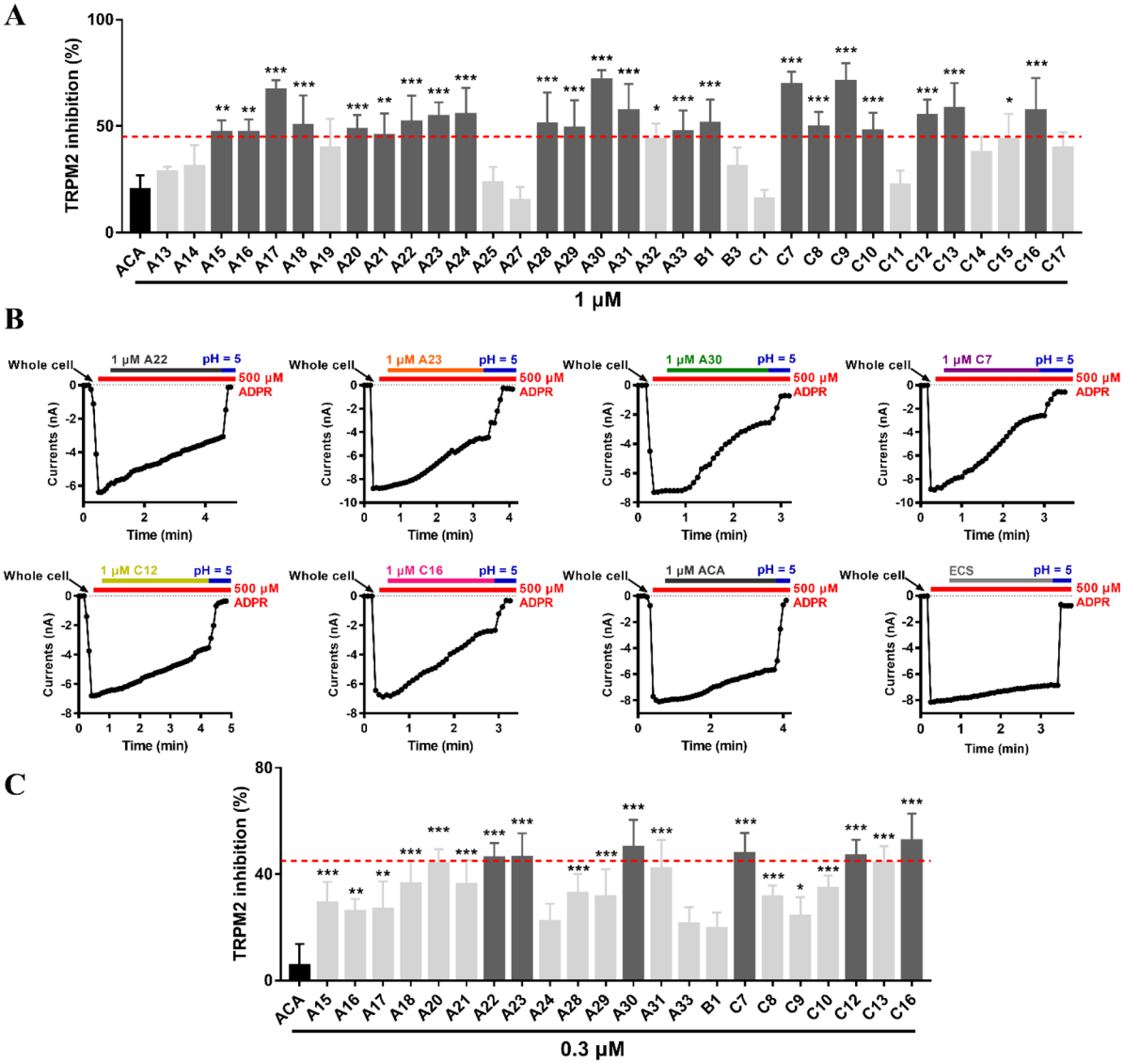

Figure 3. Inhibitory activity of selected compounds against TRPM2 currents validated by whole-cell patch-clamping. (A) Mean inhibition ratio of TRPM2 currents by 1 μM of selected compounds. (B) Representative currents of 500 μM ADPR-induced TRPM2 with treatment of 1 μM of selected compounds. (C) Mean inhibition ratio of TRPM2 currents by 0.3 μM of selected compounds. Data are presented as the mean ± SD from six independent experiments (n = 6), and ***P < 0.005, **P < 0.01, *P < 0.05, test groups compared to the ACA group, one-way ANOVA, Tukey's multiple comparison test.

than ACA was observed. However, a phenyl-substituted ACA derivative (**A13**) showed a comparable inhibitory activity (IC_{50} = 2.56 μM) when compared with ACA (IC_{50} = 3.67 μM, Figure 4). These results demonstrated that the replacement of the *n*-pentyl of ACA with phenyl was feasible for improving the potency.

To further investigate the SAR of phenyl-substituted ACA derivatives and obtain more active compounds, various substituted derivatives at the biphenyl of the compound **A13** were synthesized. The inhibitory activities of compounds that introduced methyl, methoxyl, fluorine, or trifluoromethyl into 2-, 3-, 2′-, 3′-, or 4′-positions of the biphenyl group of compound **A13** were investigated by fluorescence-based Ca^{2+} influx assays and whole-cell patch-clamp experiments (Figure 2, Figure 3, and Table S1), and they showed the following. (1) When a methyl was introduced to the 3-position (**A14**), the inhibitory activity was maintained, but the substitution of a methyl into the 2-, 2′-, 3′-, or 4′-position (**A15**, **A16**, **A20**, and **A24**) increased the inhibitory activity compared with that of ACA. (2) The introduction of a methoxyl into the 2′- or 3′-position (**A17**, **A21**) showed a higher inhibitory activity than that of ACA, whereas compound **A25** with a methoxyl substituent at the 4′-position exhibited retained potency compared with that of ACA. (3) When fluorine or trifluoromethyl was attached to the 2′- or 3′-position, the inhibitory activity was maintained (**A19**) or enhanced (**A18**, **A22**, and **A23**), particularly compounds **A22** and **A23** with a substituent at the 3′-position, with IC_{50} values of 830 and 788 nM, respectively (Figure 4). However, the substitution of fluorine and trifluoromethyl into the 4′-position decreased the inhibitory activity (**A26**, **A27**).

These results indicated that the introduction of an appropriate substituent at the 2, 2′, 3′, or 4′-position of the biphenyl group of compound **A13** could improve the inhibitory effect. Among them, the 3′-position could tolerate a more diverse modification and obtain more effective

https://doi.org/10.1021/acs.jmedchem.0c02129
J. Med. Chem. 2021, 64, 3976−3996

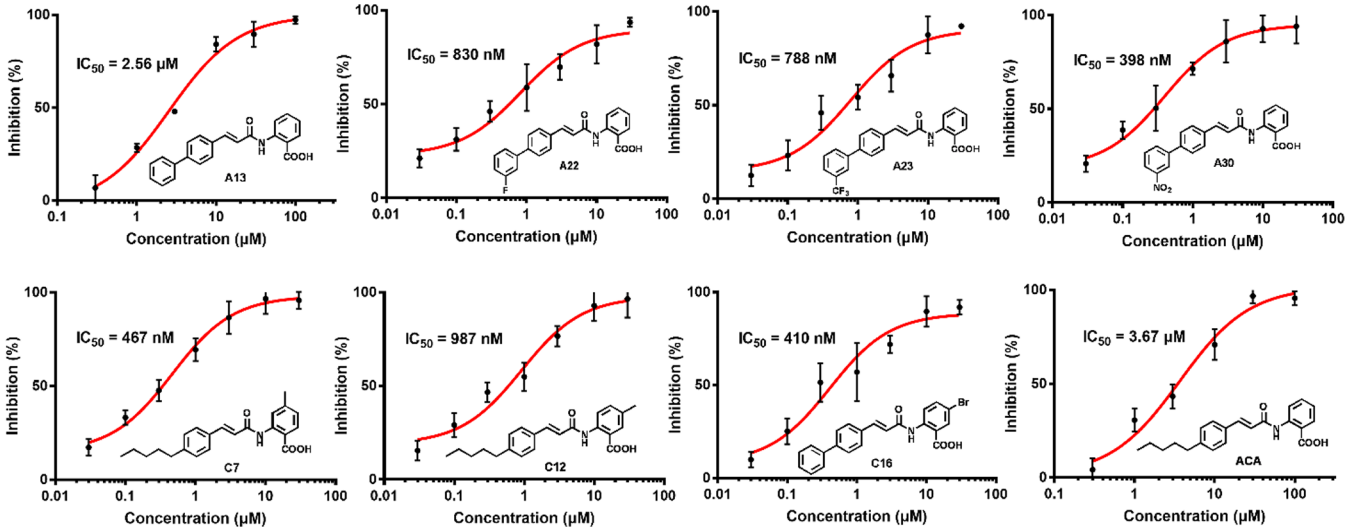

Figure 4. Dose−Response curves for **A13**, **A22**, **A23**, **A30**, **C7**, **C12**, **C16**, and **ACA**. Data are presented as the mean ± SD from six independent experiments (n = 6).

compounds than other positions, especially the substitution of fluorine and trifluoromethyl. Therefore, we synthesized and investigated the inhibitory activities of more compounds substituted at the 3′-position of the **A13** biphenyl group with a halogen or other electron-withdrawing group including chlorine, bromine, and a nitro group to discover more efficient TRPM2 inhibitors (Figure 2, Figure 3, and Table S1). Compounds **A28**−**A30** expectedly exhibited strong inhibitory activities, of which the nitro-substituted compound **A30** was the most potent TRPM2 inhibitor with an IC_{50} value of 398 nM (Figure 4). The inhibitory activity against the TRPM2 channel was enhanced with the increase of electron-withdrawing capacity of 3′-position substituents. Moreover, with the exception of compound **A24** with methyl substitution at the 4′-position, other substituents at the 4′-position (**A25**−**A27**) weakened the inhibitory activity of compound **A13**. Therefore, more alkyl groups including ethyl, isopropyl, and *tert*-butyl were introduced to the 4′-position to discover more potent compounds. For the resulting compounds (**A31**−**A33**), higher inhibitory activities were observed compared with those of ACA, especially the ethyl-substituted compound **A31**, which showed better inhibitory activity than methyl-substituted **A24**. These results indicated that the introduction of an alkyl at the 4′-position of the **A13** biphenyl group could exhibit improved inhibitory activity. In brief, a large number of resulting compounds modified on the biphenyl group of compound **A13** displayed improved or at least maintained activity. In particular, the electron-withdrawing group at the 3′-position was beneficial to increase the inhibitory activity.

The linker part of ACA consists of a carbon−carbon double bond and an amide bond. As shown in Figure 2, Figure 3, and Table S1, removing the amide bond (**B1**) resulted in improved inhibitory activity compared with ACA, whereas no inhibitory activity was observed for compound **B2**, which only removed the imine group of the amide bond. Meanwhile, the effect of removing the carbon−carbon double bond on the inhibitory activity was investigated (**B3**), which showed that the potency was retained. Then the position of the carbonyl group and the imine group in the amide bond of compound **B3** was exchanged, but decreased inhibitory activity was observed (**B4**). These results indicated that removing the carbon−carbon double bond did not affect the TRPM2 inhibitory activity, and removing amide bond was favorable to the inhibitory activity.

As indicated in Figure 2, Figure 3, and Table S1, with the removal of the carboxyl group from the 1-position to the 5- or 6-position of ACA to obtain compounds **C1** and **C2**, decreased or disappeared inhibitory activity was given, suggesting the importance of the carboxyl group at the 1-position of ACA for inhibitory activity against the TRPM2 channel. Therefore, we retained the carboxyl at the 1-position of ACA and investigated the biological activities of derivatives with the methyl or halogen group introduced at the 3-, 4-, or 5-position. When methyl or chlorine was introduced into the 3-position of ACA, the inhibitory activity was decreased or disappeared, even if the beneficial substituent was introduced into the 4- or 5-position (**C3**−**C6**). The introduction of a methyl or chlorine into the 4-position of ACA increased the inhibitory activity (**C7**, **C10**); particularly, compound **C7** with a methyl substituent showed an IC_{50} value of 467 nM (Figure 4). However, a replacement of the *n*-pentyl of **C7** and **C10** with 3′-nitrobiphenyl or biphenyl resulted in reduced inhibitory activities (**C8**, **C11**). In addition, compound **C9** with two fluorines introduced at the 4- and 5-positions of ACA showed improved inhibitory activity. For the 5-position-substituted ACA derivatives, compounds substituted with a methyl (**C12**) and bromine (**C13**) exhibited strong inhibitory activities, especially **C12** with an IC_{50} value of 987 nM (Figure 4). The replacement of the *n*-pentyl of **C13** with biphenyl or 3′-nitrobiphenyl was accompanied by the replacement of halogen-formed compounds **C14**−**C17**. Among them, biphenyl- and bromine-substituted compound **C16** was the most potent TRPM2 inhibitor with an IC_{50} value of 410 nM (Figure 4). Since derivatives of 2,3-dihydroquinazolin-4(1*H*)-one and tetrahydrocyclohepta[*c*]pyrazol were effective TRPM2 inhibitors, we also investigated the inhibitory activities of four-, six-, and seven-membered cyclic ACA derivatives formed by the carboxyl group and the ortho imine group (**C18**−**C22**). The inhibitory activity was decreased or disappeared, suggesting the importance of a free carboxyl group for the inhibitory activity. In brief, a large proportion of resulting compounds with methyl or halogen introduced at the 4- or 5-position of ACA displayed improved inhibition,

https://doi.org/10.1021/acs.jmedchem.0c02129
J. Med. Chem. 2021, 64, 3976−3996

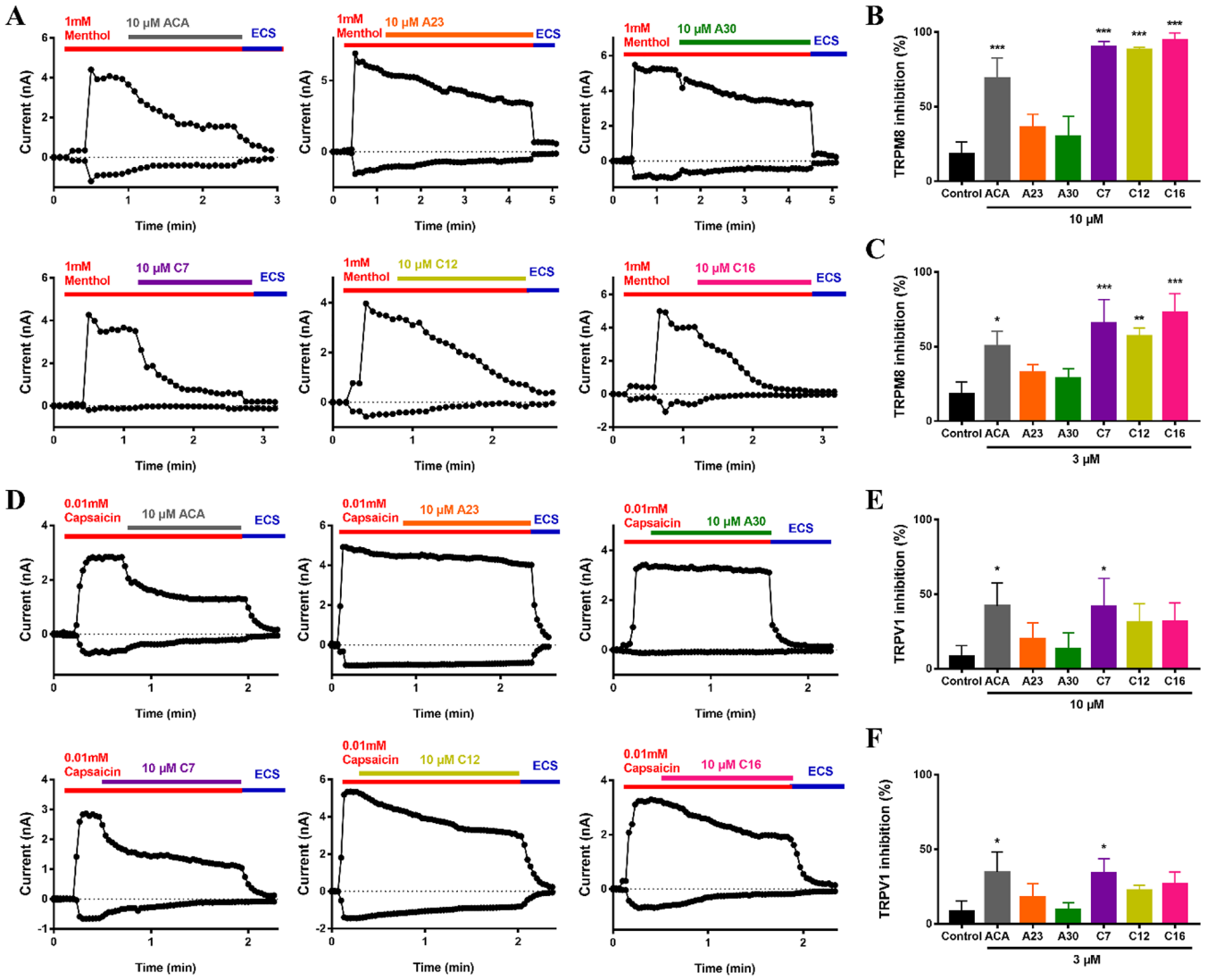

Figure 5. Selectivity evaluations of **A23**, **A30**, **C7**, **C12**, and **C16** at concentrations of 10 and 3 μM on the TRPM8 and TRPV1 channels. (A) Representative currents of 1 mM menthol-induced TRPM8 with a treatment of 10 μM compound. (B, C) Mean inhibition ratio of TRPM8 currents by 10 or 3 μM compound. (D) Representative currents of 0.01 mM capsaicin-induced TRPV1 with a treatment of 10 μM compound. (E, F) Mean inhibition ratio of TRPV1 currents by 10 or 3 μM compound. Data are presented as the mean ± SD from three to six independent experiments (n = 3−6), and ***P < 0.005, **P < 0.01, *P < 0.05, test groups compared to the control group, one-way ANOVA, Dunnett's multiple comparison test.

especially the compounds substituted with methyl and bromine.

Taken together, the structural modification of ACA resulted in a series of compounds with an improved TRPM2 inhibitory activity. Our investigation illustrated that (1) replacing the *n*-pentyl with a biphenyl group and introducing an appropriate substituent at the 2-, 2′-, 3′-, or 4′-position of the biphenyl group could improve the inhibitory effect, such as fluorine at the 2′-position, alkyl at the 4′-position, particularly electron-withdrawing groups at the 3′-position of biphenyl; (2) the removal of the amide bond of the linker part was favorable to the inhibitory activity, but the improvement was limited compared with that of Class A and Class C; (3) the introduction of a methyl and bromine into the 4- or 5-position of ACA derivatives contributed to improving inhibitory activity. Moreover, the orientation and electronegativity of the substituents on the ACA derivatives played key roles in the inhibitory activity against TRPM2. Compounds **A22**, **A23**, **A30**, **C7**, **C12**, and **C16**, which showed excellent inhibitory activities against TRPM2, were selected for further evaluation.

Inhibitory Effects of ACA Derivatives on the TRPM8 and TRPV1 Channels. Before testing the selectivity on other TRP channels, we evaluated the effect of these six compounds on the SH-SY5Y cell viability using the Cell Counting Kit-8 (CCK-8) assay. With the exception of compound **A22**, which showed 23.7% toxicity against SH-SY5Y cells at 30 μM, the other five compounds did not affect cell viability (<10% toxicity) when incubated with concentrations of 1−30 μM for 24 h (Figure S2). Therefore, we did not conduct further studies on **A22**. To evaluate the compound selectivity, the inhibitory effects of five compounds (**A23**, **A30**, **C7**, **C12**, and **C16**) on the closely related TRPM8 channel and more distantly related TRPV1 channel were investigated by whole-cell patch-clamp recordings. Menthol and capsaicin activated the TRPM8 and TRPV1 currents, respectively, in overexpressed HEK293T cells.

https://doi.org/10.1021/acs.jmedchem.0c02129
J. Med. Chem. 2021, 64, 3976−3996

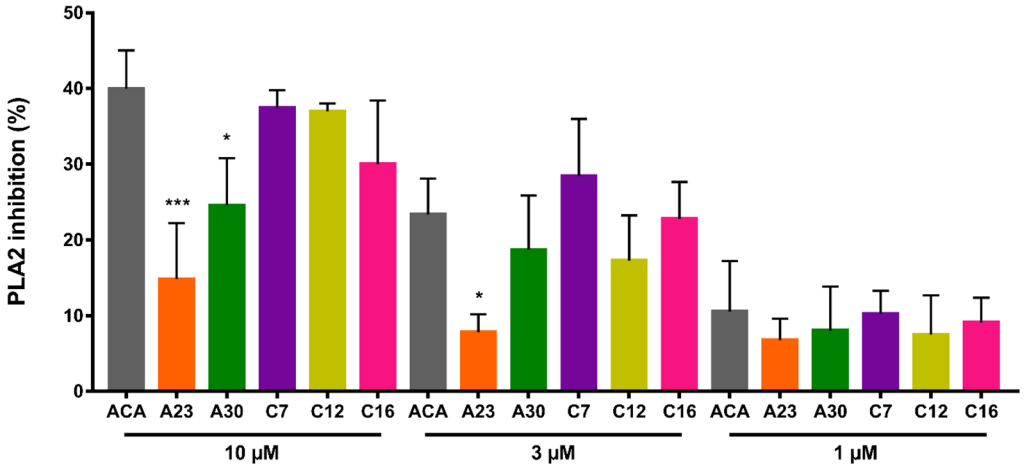

Figure 6. Inhibitory activity of **A23**, **A30**, **C7**, **C12**, and **C16** at concentrations of 10, 3, and 1 μM against PLA2. Data are presented as the mean ± SD from three determinations (n = 3), and ***P < 0.005, *P < 0.05, test groups compared to the corresponding ACA group, one-way ANOVA, Dunnett's multiple comparison test.

As indicated in Figure 5A,B, compared with the control, an extracellular addition of 10 μM **A23** and **A30** showed mild inhibitory effects on TRPM8 currents by 22.2% and 14.6%, respectively, while **C7**, **C12**, and **C16** inhibited TRPM8 currents by 88.1%, 85.6%, and 93.3%, respectively, which was even stronger than the inhibitory effect of ACA (62.2%). The effects of 3 μM compound on TRPM8 currents were tested and showed that **A23** and **A30** exhibited better specificity for the TRPM2 channel than the ACA treatment (Figure 5C). The positive control ACA showed a 39.3% inhibition ratio on TRPM8 currents at 3 μM, consistent with the reported IC_{50} value of 3.9 μM.[24] It is noteworthy that both **A23** and **A30** had an electron-withdrawing group (trifluoromethyl and nitro) at the 3′-position of biphenyl, while **C7**, **C12**, **C16** and ACA had an n-pentyl or unsubstituted biphenyl at this position, suggesting that the electron-withdrawing group at the 3′-position of biphenyl was unfavorable for the inhibition of the TRPM8 channel. In addition, **C7**, **C12**, and **C16** all had a methyl or bromine at the 4- or 5-position, which contributed to improving the inhibitory activity against the TRPM8 channel.

For the TRPV1 channel, both 10 and 3 μM **C7** resulted in a distinct reduction of TRPV1 currents compared with the control, and the other four compounds showed no significant effects on the TRPV1 currents. In particular, **A23** and **A30** only suppressed TRPV1 currents by 12.7% and 5.4%, respectively, at a concentration of 10 μM (Figure 5D−F). These results suggested that compounds containing an electron-withdrawing group at the 3′-position of biphenyl were not conducive to the inhibition of the TRPV1 channel.

Inhibitory Effects of ACA Derivatives on PLA2. As aforementioned, ACA inhibits not only TRP channels but also PLA2, which hydrolyzes cell membrane phospholipids to produce arachidonic acid (AA) and lyso-phospholipids, playing a key role in the production of inflammatory lipid mediators.[24,39,44,45] To investigate the inhibitory effects of our synthesized ACA derivatives on PLA2, the colorimetric PLA2 assay was performed on selected compounds **A23**, **A30**, **C7**, **C12**, and **C16**. As shown in Figure 6, **A23** and **A30** displayed weaker PLA2 inhibitory activities than ACA at 10 μM with 14.8% and 24.6%, respectively. The positive control ACA showed a 40.0% inhibition ratio of PLA2 at 10 μM, which was generally consistent with the reported IC_{50} value of 22 μM,[44] whereas **C7**, **C12**, and **C16** showed no significant difference in the inhibitory activity compared with ACA at a concentration of 10 μM, indicating that the selectivity of these compounds on PLA2 did not improve. At a concentration of 3 μM, only **A23** (7.8%) exhibited a lower PLA2 inhibitory activity than ACA (23.4%). It is worth noting that, at 1 μM, only a slight inhibitory activity was observed for all active compounds.

Summarizing the inhibitory activities of the most active compounds on TRP channels and PLA2, we found that different substituted groups on the ACA derivatives played critical roles in the selectivity between the TRPM2 channel and other TRP channels, as well as PLA2. Compounds with an electron-withdrawing group (trifluoromethyl and nitro) at the 3′-position of biphenyl showed specificity to the TRPM2 channel and have little or no effect on the TRPM8 and TRPV1 currents and PLA2, whereas compounds with methyl or bromine introduced at the 4- or 5-position were harmful to the specificity of the TRPM2 channel. Specifically, compounds with a methyl group at the 4- or 5-position of ACA displayed improved or retained inhibitory activity against the TRPM8 currents and PLA2. In addition, a compound with a methyl substitution at the 4-position of ACA also inhibited the TRPV1 currents. As for the replacement of n-pentyl with unsubstituted biphenyl and the introduction of a bromine at the 5-position of ACA, the compound showed an inhibitory effect on the TRPM8 currents and PLA2.

ACA Derivatives Protect SH-SY5Y Cells against OGD/R Injury. OGD/R provides a cellular model to mimic neuronal ischemia and excitotoxicity in neurodegenerative diseases such as ischemic stroke and Alzheimer's disease.[46] To confirm OGD/R-induced cell injury and evaluate the protective effects of five selected ACA derivatives, we measured the cell viability by the CCK-8 assay after OGD/R in SH-SY5Y cells. We used OGD for 8 h followed by replacement with complete culture medium for another 12 h as an OGD/R model, and edaravone (EDA), an ROS scavenger that was widely used clinically as a neuroprotectant for the treatment of cerebral infarction, was selected as the positive control. The results showed that the cell viability was obviously decreased to 49.4% in the OGD/R group compared with the control group, and 1−30 μM EDA exhibited efficient protective effects on SH-SY5Y cells; in particular, 3 μM EDA mediated the high upregulation of cell

https://doi.org/10.1021/acs.jmedchem.0c02129
J. Med. Chem. 2021, 64, 3976−3996

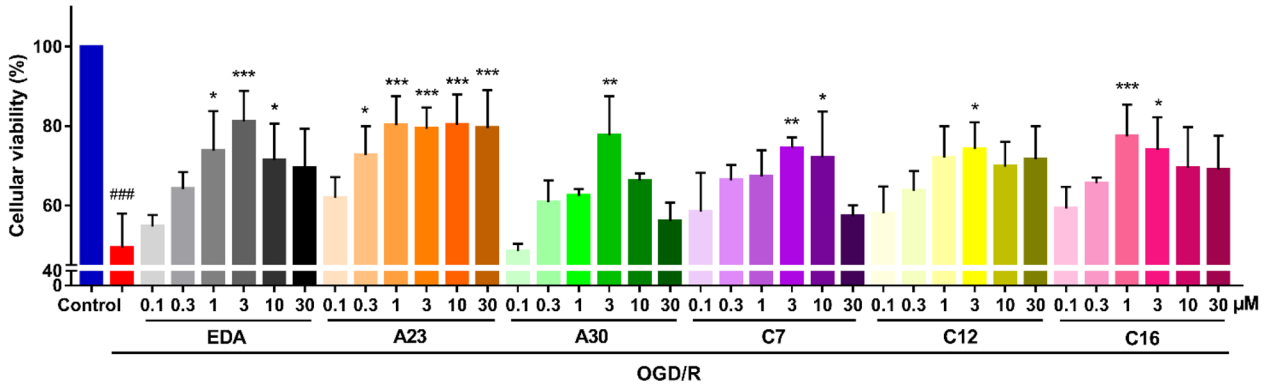

Figure 7. SH-SY5Y cell injury induced by OGD/R and the protective effects of ACA derivatives. Data are presented as the mean ± SD from three independent experiments (n = 3), and $^{###}P < 0.005$, OGD/R group compared to the control group; $^{***}P < 0.005$, $^{**}P < 0.01$, $^{*}P < 0.05$, test groups compared to the OGD/R group, one-way ANOVA, Tukey's multiple comparison test.

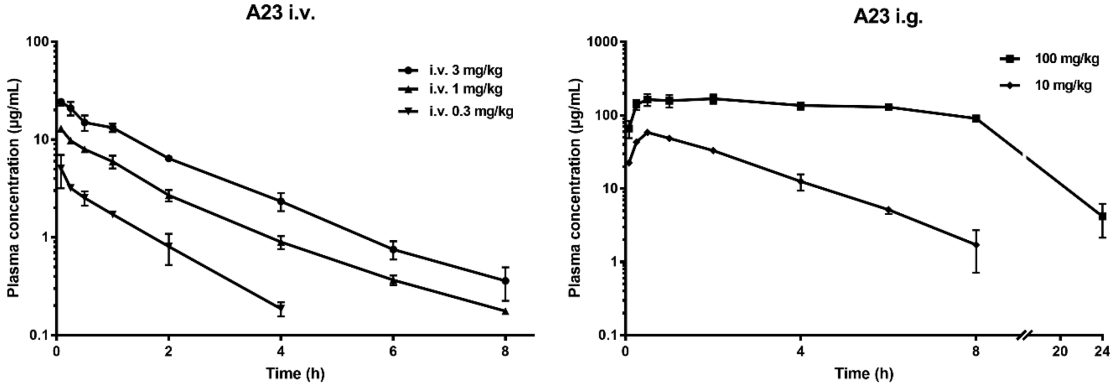

Figure 8. Plasma concentration−time profiles for **A23** i.v. (0.3, 1, and 3 mg/kg) and i.g. (10, 100 mg/kg) administration in mice. Data are presented as the mean ± SD, and each measurement was repeated three times (n = 3).

Table 1. PK Parameters of A23 in Mice Plasma after Single-Dose Intravenous and Intragastric Administration[a]

route	dose (mg/kg)	$T_{1/2}$ (h)	T_{max} (h)	C_{max} (μg/mL)	AUC_{0-t} (h·μg/mL)	$AUC_{0-\infty}$ (h·μg/mL)	CL (mL/h/kg)	MRT (h)	F%-0.3 mg/kg	F%-1 mg/kg
i.v.	0.3	0.93	0.08	5.07	5.20	5.45	55.0	1.19		
i.v.	1	1.70	0.08	12.95	18.46	18.89	52.9	1.70		
i.g.	10	1.42	0.50	58.35	156.63	160.13	62.5	2.25	90.4	84.8

[a]Each measurement was repeated three times (n = 3).

viability to 81.2% (Figure 7). Compounds **A23**, **A30**, **C7**, **C12**, and **C16** showed comparable protective activities with EDA at a concentration of 3 μM compared with the OGD/R group. Among them, **A23** displayed considerable protective activities when the concentration was only 0.3 μM (68.7%), and **A23** induced an increase of cell viability to 80% at a wider range of concentrations (1, 3, 10, and 30 μM) compared with EDA (3 μM). These results demonstrated that all five compounds at a certain concentration exhibited a protective effect on the cell viability of SH-SY5Y cells subjected to OGD/R; especially, compound **A23** had a wider effective concentration range, which was between 0.3 and 30 μM.

Besides the administration of EDA, **A30** and **C7** at 10 and 30 μM displayed some degree of cytotoxicity to SH-SY5Y cells under a pathological condition (OGD/R), whereas these compounds did not affect the cell viability under normoxic and normal sugar conditions (Figure S1). Similar phenomena have been reported in some literature, including EDA and other neuroprotective agents.[47−49] The reason and mechanism are still unclear and remain to be further studied.

PK Studies of A23 In Vivo. On the basis of its favorable specificity to the TRPM2 channel as well as protective activity in vitro, **A23** was further evaluated in in vivo PK studies. After a single intravenous (i.v.) administration with 3 mg/kg and a single intragastric (i.g.) administration with 100 mg/kg, the half-life ($T_{1/2}$), maximum concentration (C_{max}), and area under the curve ($AUC_{0-\infty}$) were determined to be 1.34 h, 24.33 μg/mL, 40.93 h·μg/mL and 3.62 h, 168.17 μg/mL, 1872.62 h·μg/mL, respectively (Figure 8 and Table S2). There were no apparent adverse effects observed in mice at a high gavage dose of 100 mg/kg. However, the oral bioavailability (F%) of **A23** was calculated to be greater than 100%, which suggested that the doses may be outside the linear pharmacokinetic range.

Subsequently, the single administered dose was reduced to 0.3 (i.v.), 1 (i.v.), and 10 mg/kg (i.g.), and the plasma concentration−time profiles and key PK parameters are summarized in Figure 8 and Table 1. The results indicated that the PK behavior of **A23** for the i.v. (0.3 and 1 mg/kg) and i.g. (10 mg/kg) administration conformed to the one-compartment model. After single 0.3 and 1 mg/kg i.v. doses

https://doi.org/10.1021/acs.jmedchem.0c02129
J. Med. Chem. 2021, 64, 3976−3996

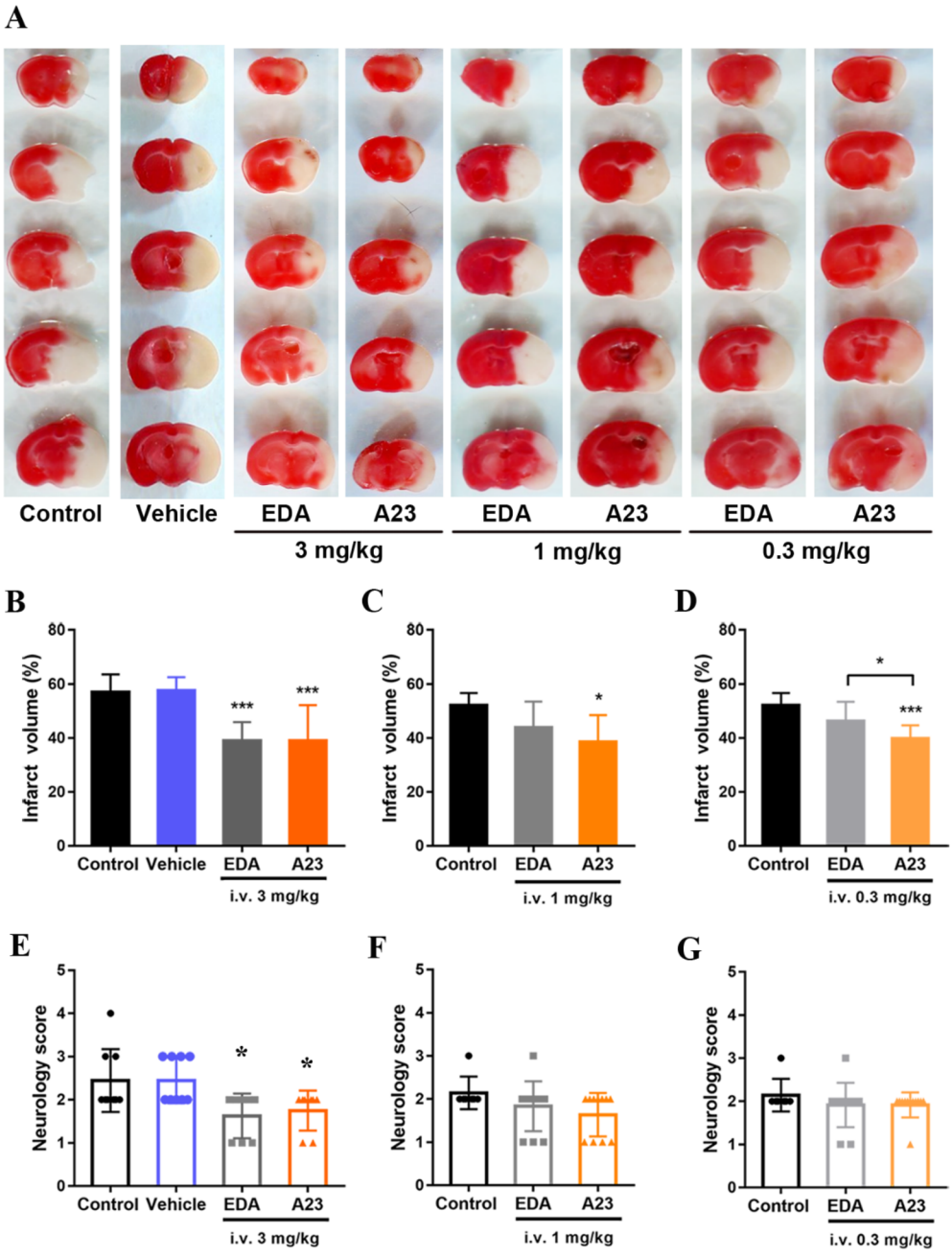

Figure 9. Effects of **A23** and EDA i.v. administration (3, 1, and 0.3 mg/kg) 24 h after tMCAO in mice. (A) Representative TTC-stained brain slices of mice intravenous in the control, vehicle, EDA, and **A23** (0.3, 1, and 3 mg/kg) treatment groups; magenta: healthy tissue, white: damaged tissue. (B–D) Statistical analysis of the percentage of infarct volume after tMCAO in the control, vehicle, and 3 (B), 1 (C), and 0.3 (D) mg/kg EDA and **A23** treatment groups. (E–G) Statistical analysis of the neurological scores after tMCAO in the control, vehicle, and 3 (E), 1 (F), and 0.3 (G) mg/kg EDA and **A23** treatment groups. Data are presented as the mean ± SD, and each measurement was repeated 7–12 times (n = 7–12), and ***P < 0.005, *P < 0.05, one-way ANOVA, Tukey's multiple comparison test.

of **A23**, the $T_{1/2}$, clearance rate (CL), and mean residence time (MRT) values were 0.93 h, 55.0 mL/h/kg, 1.19 and 1.70 h, 52.9 mL/h/kg, and 1.70 h, respectively. At a dose of 10 mg/kg i.g., **A23** was rapidly absorbed with a time-to-maximum-concentration (T_{max}) of 0.5 h, a $T_{1/2}$ of 1.42 h, and an MRT of 2.25 h. These results showed that compound **A23** was rapidly distributed and eliminated, and the clearance of **A23** was in an acceptable range. **A23** had high plasma exposure with high C_{max} and $AUC_{0-\infty}$. When **A23** was administrated by the i.v. route at only 0.3 mg/kg, the time for the effective concentration to be higher than the IC_{50} value of TRPM2 (0.32 μg/mL) could reach 2–4 h (the concentration of **A23** at 2h was 0.81 μg/mL). Furthermore, the oral bioavailability of **A23** with 10 mg/kg (i.g.) administration was 90.4% (calculated by i.v. 0.3 mg/kg $AUC_{0\text{-}t\_D}$) and 84.8% (calculated by i.v. 1 mg/kg $AUC_{0\text{-}t\_D}$), respectively. Overall, compound **A23** appeared to have favorable drug-like PK properties.

A23 Treatment Provides Neuroprotection following Focal Cerebral Ischemia in Mice. Encouraged by its excellent PK profiles, we studied compound **A23** in an in vivo tMCAO model. Mice were subjected to 90 min of tMCAO, and control (saline), vehicle (5% dimethyl sulfoxide

https://doi.org/10.1021/acs.jmedchem.0c02129
J. Med. Chem. 2021, 64, 3976–3996

(DMSO)/5% Solutol in saline), EDA (3, 1, and 0.3 mg/kg, i.v.), or **A23** (3, 1, and 0.3 mg/kg, i.v.) was administered at 3 h after the onset of reperfusion. As shown in Figure 9A, the infarct volume was calculated using 2,3,5-triphenyltetrazolium chloride (TTC) staining on 1 mm brain sections 24 h after tMCAO. A considerable reduction in the infarct volume was observed with a treatment of 3 mg/kg EDA (39.0 ± 2.4%, n = 8, $p < 0.005$) and 3 mg/kg **A23** (38.9 ± 4.7%, n = 8, $p < 0.005$) compared with the vehicle group (57.6 ± 4.9%, n = 9), whereas there was no difference in infarct volume in the 3 mg/kg EDA- and 3 mg/kg **A23**-treated groups (Figure 9B). Considering the high plasma exposure of **A23** at low doses, the effects of 1 and 0.3 mg/kg **A23** on I/R injury following tMCAO were further investigated. The results showed that the 1 mg/kg EDA-treated group (43.9 ± 2.8%, n = 12) and 0.3 mg/kg EDA-treated group (46.2 ± 2.1%, n = 12) did not significantly decrease the infarct volume compared with the control group (52.0 ± 1.7%, n = 7). However, an obvious alleviation in infarct volume was observed in both the 1 mg/kg **A23**-treated group (38.5 ± 2.8%, n = 12, $p < 0.05$) and 0.3 mg/kg **A23**-treated groups (39.8 ± 1.4%, n = 12, $p < 0.005$) compared to the control group (52.0 ± 1.7%, n = 7), consistent with the PK results. Notably, at 0.3 mg/kg, compound **A23** was significantly more effective than EDA in reducing the infarct volume (39.8 ± 1.4% vs 46.2 ± 2.1%, n = 12, $p < 0.05$) (Figure 9C,D). Collectively, the infarct volume of mice in the EDA (3 mg/kg) group and **A23** (3, 1, and 0.3 mg/kg) group was significantly improved compared to that of the vehicle-treated group, and the effect of **A23** (0.3 mg/kg) was preferable to that of EDA (0.3 mg/kg).

To assess the health of the mouse, we evaluated neurological scores at 24 h after tMCAO. As shown in Figure 9E, the scores obtained in the groups treated with 3 mg/kg EDA (1.6 ± 0.2, n = 8, $p < 0.05$) and 3 mg/kg **A23** (1.8 ± 0.2, n = 8, $p < 0.05$) were both markedly lower than those of the vehicle-treated group (2.4 ± 0.5, n = 9), illustrating that **A23** had the same effect as EDA in reducing neurological scores. Neither EDA nor **A23** at a dose of 1 and 0.3 mg/kg showed significantly different neurological improvements compared with the control group (Figure 9F,G). Taken together, compound **A23** showed protective effects against a cerebral infarction induced by focal cerebral ischemia in mice, which were equal to or even better than the positive control EDA, suggesting that **A23** is an attractive candidate for the intervention of ischemic stroke and merits further study.

CONCLUSION

We designed and synthesized 59 novel ACA derivatives to discover more potent and selective TRPM2 inhibitors. Some of them exhibited a stronger inhibitory activity against the TRPM2 currents than ACA, particularly compounds **A22**, **A23**, **A30**, **C7**, **C12**, and **C16**, with IC_{50} values ranging from 398 to 987 nM. More importantly, **A23** showed TRPM2 selectivity over TRPM8 and TRPV1 channels as well as PLA2. SAR studies revealed that compounds containing electron-withdrawing groups at the 3′-position of biphenyl improved the potency and specificity of the TRPM2 channel, while compounds with a methyl or bromine introduced at the 4- or 5-position contributed to improving inhibitory activity but were harmful to the specificity of the TRPM2 channel. These summarized SARs provide valuable insights for the further development of specific TRPM2 inhibitors. Compound **A23** exhibited excellent neuroprotective activities both in the in vitro OGD/R model and in the in vivo tMCAO model, which were equal to or even better than the widely used neuroprotectant EDA. Furthermore, the PK studies showed that **A23** exhibited high plasma exposure, which was consistent with the pharmacodynamic results. Overall, **A23**, as a potent and selective TRPM2 inhibitor with neuroprotective activity in vitro and anticerebral infarction efficacy in vivo, might serve as a useful molecular tool for further physiology and pathophysiology function studies related to the TRPM2 channel and also lead to potential clinical therapeutic agents for ischemic injury.

EXPERIMENTAL SECTION

Materials and Methods. All of the chemicals and solvents used were obtained from commercial sources. The solvents were dried by standard procedures. Thin-layer chromatography (Silica gel GF254, Qingdao Haiyang Chemical Co., Ltd.) was employed to monitor the reaction progress, and silica column chromatography was performed to purify the crude product (silica gel 200−300 mesh, Shanghai Sanpont Co., Ltd.). ^{1}H NMR spectra and ^{13}C NMR spectra were recorded at 400 MHz using a Bruker Avance III spectrometer (Bruker Co.) in a $CDCl_3$ or DMSO-d_6 solution with tetramethylsilane as the internal standard, and chemical shift values were given in parts per million. The NMR data were processed by the software MestReNova (ver. 6.1.0, mestrelab research S.L.). The splitting peak was designated as s, singlet; d, doublet; dd, double doublet; t, triplet; m, multiplet; br, broad. The high-resolution mass spectrometry (HRMS) was measured on an FT-MS-Bruker APEX IV mass spectrometer. The purity of all final compounds for biological tests was determined to be greater than 95% with a high-performance liquid chromatography (HPLC) analysis (Dione HPLC system consisting of LPG-3400SD pump and DAD-3000 UV detector). Water was used with 0.1% formic acid as mobile phase A (2−20%), acetonitrile was mobile phase B (80−98%); Diamonsil C18 column, 5 μm, 4.6 × 250 mm, 25 °C, 1 mL/min was used.

Chemical Synthesis. *General Procedure for the Synthesis of Compounds 3a−3n.* Methyl 2-aminobenzoate **10** (604 mg, 4 mmol) and sodium hydroxide (480 mg, 12 mmol) were dissolved in H_2O (6 mL), ethanol (6 mL), and tetrahydrofuran (THF) (18 mL). The reaction mixture was refluxed for 4 h, and the solvent was removed under reduced pressure. The residue was extracted with ethyl acetate (EtOAc) twice. The water layer was neutralized with 1 N HCl, and the resulting precipitate was filtered and dried to afford 2-aminobenzoic acid **11a**. A mixture of 2-aminobenzoic acid **11a** or commercially available aminobenzoic acid derivatives **11b−11n** (4 mmol) and 2,2-dimethyl-1,3-dioxane-4,6-dione (576 mg, 4 mmol) in toluene (5 mL) was refluxed for 3 h. The suspension was cooled, filtered, washed with toluene, and dried to afford carboxyacetamidobenzoic acid derivatives **12a−12n**.[40]

*General Procedure for the Synthesis of Compounds **6a−6t**.* $Pd(PPh_3)_4$ (147 mg, 0.13 mol) was added to a degassed mixture of substituted benzboric acids **13a−13s** (1.81 mmol), 4-bromobenzaldehyde derivatives **14a−14c** (1.27 mmol), K_2CO_3 (501 mg, 3.63 mmol) in dioxane (4 mL), and water (2 mL) under argon. The mixture was heated at 105 °C for 24 h, cooled to room temperature (rt), and extracted with EtOAc three times. The combined organic layers were washed with brine, dried over anhydrous Na_2SO_4, filtered, and concentrated under reduced pressure. The crude product was purified by silica gel column chromatography eluting with petroleum ether (PE)/EtOAc (6/1) to afford biphenylcarbaldehyde derivatives **15a−15t**.[28]

General Procedure for the Synthesis of Compounds A1−A33, C1−C17. Piperidine (94 mg, 1.1 mmol) was added to a suspension of biphenylcarbaldehyde derivatives **15a−15t** or commercially available benzaldehyde derivatives **16a−16m** (1.1 mmol) and carboxyacetamidobenzoic acid derivatives **12a−12n** (1 mmol) in toluene (3 mL). The mixture was heated to reflux for 4 h, followed by being stirred at room temperature for an additional 1 h and then acidified with 1 N HCl. Subsequently, the mixture was extracted with EtOAc three times. The combined organic layers were washed with brine, dried

https://doi.org/10.1021/acs.jmedchem.0c02129
J. Med. Chem. 2021, 64, 3976−3996

over anhydrous Na_2SO_4, filtered, and concentrated under reduced pressure. The crude product was purified by silica gel column chromatography eluting with dichloromethane (DCM)/methanol (MeOH) (100/3) to afford **A1**−**A33** and **C1**−**C17**.[40]

(E)-2-(3-Phenylacrylamido)benzoic Acid (A1). Off-white solid. Yield: 62%. mp 198−200 °C. ^{1}H NMR (400 MHz, $CDCl_3$) δ 11.30 (s, 1H), 8.94 (d, J = 9.0 Hz, 1H), 8.22 (d, J = 7.6 Hz, 1H), 7.83 (d, J = 15.6 Hz, 1H), 7.67 (t, J = 17.2 Hz, 1H), 7.60 (d, J = 4.0 Hz, 2H), 7.41−7.40 (m, 3H), 7.18 (t, J = 7.6 Hz, 1H), 6.65 (d, J = 15.6 Hz, 1H). ^{13}C NMR (101 MHz, DMSO-d_6) δ 172.2, 165.0, 142.9, 142.2, 135.7, 134.6, 131.9, 130.2, 128.9, 128.1, 122.9, 121.7, 120.9, 114.2. HRMS (electrospray ionization time-of-flight (ESI-TOF$^-$)) calcd for $C_{16}H_{12}NO_3$ [M-H]$^-$ m/z 266.0817, found 266.0816.

(E)-2-(3-(4-Chlorophenyl)acrylamido)benzoic Acid (A2). Off-white solid. Yield: 64%. mp 223−225 °C. ^{1}H NMR (400 MHz, DMSO-d_6) δ 13.63 (s, 1H), 11.35 (s, 1H), 8.61 (d, J = 8.4 Hz, 1H), 8.02 (d, J = 7.8 Hz, 1H), 7.79 (d, J = 8.3 Hz, 2H), 7.65−7.61 (m, 2H), 7.51 (d, J = 8.3 Hz, 2H), 7.19 (t, J = 7.6 Hz, 1H), 6.94 (d, J = 15.6 Hz, 1H). ^{13}C NMR (101 MHz, DMSO-d_6) δ 169.9, 164.1, 141.2, 140.4, 135.0, 134.5, 133.9, 131.6, 130.4, 129.4, 123.7, 123.4, 120.9, 117.4. HRMS (ESI-TOF$^-$) calcd for $C_{16}H_{11}NO_3Cl$ [M-H]$^-$ m/z 300.0427, found 300.0427.

(E)-2-(3-(p-Tolyl)acrylamido)benzoic Acid (A3). Off-white solid. Yield: 65%. mp 199−201 °C. ^{1}H NMR (400 MHz, DMSO-d_6) δ 13.63 (s, 1H), 11.34 (s, 1H), 8.61 (d, J = 8.4 Hz, 1H), 8.01 (d, J = 7.8 Hz, 1H), 7.65−7.58 (m, 4H), 7.26 (d, J = 7.8 Hz, 2H), 7.18 (t, J = 7.6 Hz, 1H), 6.83 (d, J = 15.6 Hz, 1H), 2.35 (s, 3H). ^{13}C NMR (101 MHz, DMSO-d_6) δ 170.0, 164.4, 141.8, 141.4, 140.4, 134.4, 132.1, 131.6, 130.0, 128.6, 123.2, 121.8, 120.8, 117.3, 21.4. HRMS (ESI-TOF$^-$) calcd for $C_{17}H_{14}NO_3$ [M-H]$^-$ m/z 280.0974, found 280.0974.

(E)-2-(3-(4-Ethylphenyl)acrylamido)benzoic Acid (A4). Off-white solid. Yield: 51%. mp 176−178 °C. ^{1}H NMR (400 MHz, DMSO-d_6) δ 13.62 (s, 1H), 11.34 (s, 1H), 8.61 (d, J = 8.4 Hz, 1H), 8.01 (d, J = 8.7 Hz, 1H), 7.67−7.59 (m, 4H), 7.29 (d, J = 7.3 Hz, 2H), 7.18 (t, J = 5.9 Hz, 1H), 6.83 (d, J = 15.4 Hz, 1H), 2.66 (q, J = 15.2 Hz, 2H), 1.21 (t, J = 15.1, 3H). ^{13}C NMR (101 MHz, DMSO-d_6) δ 170.0, 164.4, 146.6, 141.8, 141.4, 134.4, 132.4, 131.6, 128.8, 128.7, 123.3, 121.9, 120.8, 117.3, 28.5, 15.8. HRMS (ESI-TOF$^-$) calcd for $C_{18}H_{16}NO_3$ [M-H]$^-$ m/z 294.1130, found 294.1126.

(E)-2-(3-(4-Propylphenyl)acrylamido)benzoic Acid (A5). Off-white solid. Yield: 51%. mp 117−119 °C. ^{1}H NMR (400 MHz, DMSO-d_6) δ 13.61 (br s, 1H), 11.34 (s, 1H), 8.62 (d, J = 8.4 Hz, 1H), 8.01 (d, J = 7.7 Hz, 1H), 7.65−7.59 (m, 4H), 7.26 (d, J = 7.8 Hz, 2H), 7.18 (t, J = 7.4 Hz, 1H), 6.83 (d, J = 15.6 Hz, 1H), 2.58 (t, J = 7.4 Hz, 2H), 1.65−1.55 (m, 2H), 0.89 (t, J = 7.3 Hz, 3H). ^{13}C NMR (101 MHz, DMSO-d_6) δ 169.9, 164.4, 145.0, 141.8, 141.4, 134.5, 132.4, 131.6, 129.4, 128.7, 123.3, 121.8, 120.9, 117.3, 37.6, 24.3, 14.1. HRMS (ESI-TOF$^-$) calcd for $C_{19}H_{18}NO_3$ [M-H]$^-$ m/z 308.1287, found 308.1289.

(E)-2-(3-(4-Isopropylphenyl)acrylamido)benzoic Acid (A6). Off-white solid. Yield: 58%. mp 162−164 °C. ^{1}H NMR (400 MHz, DMSO-d_6) δ 11.36 (s, 1H), 8.62 (d, J = 8.2 Hz, 1H), 8.02 (dd, J = 7.9, 1.3 Hz, 1H), 7.66−7.62 (m, 3H), 7.60−7.59 (m, 1H), 7.31 (d, J = 8.1 Hz, 2H), 7.18 (t, J = 7.2 Hz, 1H), 6.82 (d, J = 15.6 Hz, 1H), 2.97−2.87 (m, 1H), 1.21 (d, J = 6.9 Hz, 6H). ^{13}C NMR (101 MHz, DMSO-d_6) δ 170.1, 164.3, 151.1, 141.8, 141.5, 134.4, 132.5, 131.6, 128.7, 127.3, 123.2, 121.9, 120.8, 117.1, 33.8, 24.0. HRMS (ESI-TOF$^-$) calcd for $C_{19}H_{18}NO_3$ [M-H]$^-$ m/z 308.1287, found 308.1284.

(E)-2-(3-(4-(tert-Butyl)phenyl)acrylamido)benzoic Acid (A7). Off-white solid. Yield: 46%. mp 191−193 °C. ^{1}H NMR (400 MHz, DMSO-d_6) δ 11.36 (s, 1H), 8.62 (d, J = 8.3 Hz, 1H), 8.02 (dd, J = 7.9, 1.3 Hz, 1H), 7.67−7.59 (m, 4H), 7.45 (d, J = 8.4 Hz, 2H), 7.20−7.16 (m, 1H), 6.83 (d, J = 15.6 Hz, 1H), 1.29 (s, 9H). ^{13}C NMR (101 MHz, DMSO-d_6) δ 170.0, 164.3, 153.3, 141.7, 141.5, 134.5, 132.1, 131.6, 128.5, 126.2, 123.2, 122.0, 120.8, 117.1, 35.0, 31.4. HRMS (ESI-TOF$^-$) calcd for $C_{20}H_{20}NO_3$ [M-H]$^-$ m/z 322.1443, found 322.1443.

(E)-2-(3-(4-Methoxyphenyl)acrylamido)benzoic Acid (A8). Off-white solid. Yield: 57%. mp 164−166 °C. ^{1}H NMR (400 MHz, DMSO-d_6) δ 13.64 (s, 1H), 11.31 (s, 1H), 8.63 (d, J = 8.4 Hz, 1H), 8.01 (d, J = 7.8 Hz, 1H), 7.70−7.57 (m, 4H), 7.17 (t, J = 7.5 Hz, 1H), 6.98 (d, J = 8.6 Hz, 2H), 6.73 (d, J = 15.6 Hz, 1H), 4.09 (q, J = 7.0 Hz, 2H), 1.35 (t, J = 6.9 Hz, 3H). ^{13}C NMR (101 MHz, DMSO-d_6) δ 170.0, 164.6, 160.6, 141.7, 141.5, 134.5, 131.6, 130.4, 127.3, 123.2, 120.8, 120.1, 117.1, 115.2, 63.7, 15.0. HRMS (ESI-TOF$^-$) calcd for $C_{18}H_{16}NO_4$ [M-H]$^-$ m/z 310.1079, found 310.1075.

(E)-2-(3-(4-(Isopropylcarbamoyl)phenyl)acrylamido)benzoic Acid (A9). Off-white solid. Yield: 58%. mp 236−238 °C. ^{1}H NMR (400 MHz, DMSO-d_6) δ 12.37 (s, 1H), 8.62 (d, J = 7.9 Hz, 1H), 8.30 (d, J = 7.6 Hz, 1H), 8.05 (d, J = 7.4 Hz, 1H), 7.89 (d, J = 7.9 Hz, 2H), 7.79 (d, J = 7.6 Hz, 2H), 7.64 (d, J = 15.7 Hz, 1H), 7.54 (t, J = 7.6 Hz, 1H), 7.14 (t, J = 7.4 Hz, 1H), 6.93 (d, J = 15.7 Hz, 1H), 4.15−4.06 (m, 1H), 1.18 (d, J = 6.5 Hz, 6H). ^{13}C NMR (101 MHz, DMSO-d_6) δ 170.5, 165.2, 163.9, 141.2, 140.3, 137.3, 136.1, 133.3, 131.7, 128.3, 128.2, 124.8, 123.1, 120.3, 119.8, 41.5, 22.8. HRMS (ESI-TOF$^-$) calcd for $C_{20}H_{19}N_2O_4$ [M-H]$^-$ m/z 351.1345, found 351.1343.

(E)-2-(3-(4-(Pyridin-3-yl)phenyl)acrylamido)benzoic Acid (A10). Off-white solid. Yield: 61%. mp 256−258 °C. ^{1}H NMR (400 MHz, DMSO-d_6) δ 12.66 (br s, 1H), 8.96 (s, 1H), 8.64−8.60 (m, 2H), 8.14 (d, J = 7.9 Hz, 1H), 8.05 (d, J = 7.6 Hz, 1H), 7.86−7.80 (m, 4H), 7.67 (d, J = 15.7 Hz, 1H), 7.53−7.50 (m, 2H), 7.12 (t, J = 7.6 Hz, 1H), 6.90 (d, J = 15.7 Hz, 1H). ^{13}C NMR (101 MHz, DMSO-d_6) δ 170.7, 164.0, 149.3, 148.1, 141.2, 140.4, 138.7, 135.2, 134.8, 134.5, 133.1, 131.8, 129.3, 127.7, 124.4, 123.9, 122.9, 120.2, 43.9, 22.6, 22.2. HRMS (ESI-TOF$^-$) calcd for $C_{21}H_{15}N_2O_3$ [M-H]$^-$ m/z 343.1083, found 343.1081.

(E)-2-(3-(4-(Piperidin-1-yl)phenyl)acrylamido)benzoic Acid (A11). Brown solid. Yield: 61%. mp 215−217 °C. ^{1}H NMR (400 MHz, DMSO-d_6) δ 13.58 (br s, 1H), 11.27 (s, 1H), 8.64 (d, J = 8.4 Hz, 1H), 8.01 (d, J = 7.6 Hz, 1H), 7.63−7.50 (m, 4H), 7.16 (t, J = 7.5 Hz, 1H), 6.94 (d, J = 8.6 Hz, 2H), 6.60 (d, J = 15.5 Hz, 1H), 3.28 (s, 4H), 1.58 (s, 6H). ^{13}C NMR (101 MHz, DMSO-d_6) δ 170.0, 164.9, 152.8, 142.2, 141.8, 134.4, 131.6, 130.1, 123.9, 122.9, 120.6, 117.8, 116.9, 115.0, 48.8, 25.4, 24.4. HRMS (ESI-TOF$^-$) calcd for $C_{21}H_{21}N_2O_3$ [M-H]$^-$ m/z 349.1552, found 349.1549.

(E)-2-(3-(4-Morpholinophenyl)acrylamido)benzoic Acid (A12). Yellow solid. Yield: 59%. mp 239−241 °C. ^{1}H NMR (400 MHz, DMSO-d_6) δ 13.61 (s, 1H), 11.29 (s, 1H), 8.65 (d, J = 8.3 Hz, 1H), 8.02 (d, J = 7.7 Hz, 1H), 7.63−7.53 (m, 4H), 7.16 (t, J = 7.5 Hz, 2H), 6.96 (d, J = 8.4 Hz, 1H), 6.64 (d, J = 15.5 Hz, 1H), 3.73 (s, 4H), 3.21 (s, 4H). ^{13}C NMR (101 MHz, DMSO-d_6) δ 170.0, 164.8, 152.6, 142.1, 141.7, 134.5, 131.6, 130.0, 125.1, 123.0, 120.7, 118.5, 116.9, 114.8, 66.4, 47.8. HRMS (ESI-TOF$^-$) calcd for $C_{20}H_{19}N_2O_4$ [M-H]$^-$ m/z 351.1345, found 351.1342.

(E)-2-(3-([1,1′-Biphenyl]-4-yl)acrylamido)benzoic Acid (A13). Off-white solid. Yield: 66%. mp 248−250 °C. ^{1}H NMR (400 MHz, DMSO-d_6) δ 11.39 (s, 1H), 8.65 (d, J = 8.2 Hz, 1H), 8.04 (d, J = 7.6 Hz, 2H), 7.83 (d, J = 7.8 Hz, 2H), 7.75−7.72 (m, 4H), 7.67−7.62 (m, 2H), 7.50 (t, J = 15.2 Hz, 2H), 7.40 (t, J = 17.2 Hz, 1H), 7.20 (t, J = 16.4 Hz, 1H), 6.94 (d, J = 15.6 Hz, 1H). ^{13}C NMR (101 MHz, DMSO-d_6) δ 169.9, 164.3, 142.0, 141.3, 139.8, 134.4, 134.1, 131.6, 129.5, 129.3, 128.4, 127.6, 127.2, 123.4, 122.9, 120.9, 117.5, 117.4. HRMS (ESI-TOF$^-$) calcd for $C_{22}H_{16}NO_3$ [M-H]$^-$ m/z 342.1130, found 342.1130.

(E)-2-(3-(3-Methyl-[1,1′-biphenyl]-4-yl)acrylamido)benzoic Acid (A14). Off-white solid. Yield: 39%. mp 223−225 °C. ^{1}H NMR (400 MHz, DMSO-d_6) δ 13.75 (br s, 1H), 8.64 (d, J = 7.8 Hz, 1H), 8.10 (d, J = 5.5 Hz, 1H), 7.83 (d, J = 15.4 Hz, 1H), 7.75−7.67 (m, 3H), 7.57 (s, 1H), 7.47−7.38 (m, 5H), 7.03 (s, 1H), 6.71 (d, J = 15.5 Hz, 1H), 2.47 (s, 3H). ^{13}C NMR (101 MHz, DMSO-d_6) δ 171.4, 163.8, 141.4, 141.3, 139.8, 138.1, 137.2, 132.9, 131.9, 131.6, 129.4, 129.3, 128.2, 127.2, 127.0, 125.0, 124.8, 122.3, 119.3, 110.0, 20.0. HRMS (ESI-TOF$^-$) calcd for $C_{23}H_{18}NO_3$ [M-H]$^-$ m/z 356.1287, found 356.1284.

(E)-2-(3-(2-Methyl-[1,1′-biphenyl]-4-yl)acrylamido)benzoic Acid (A15). Off-white solid. Yield: 42%. mp 187−189 °C. ^{1}H NMR (400 MHz, DMSO-d_6) δ 13.68 (br s, 1H), 11.39 (s, 1H), 8.64 (d, J = 8.3 Hz, 1H), 8.02 (d, J = 7.8 Hz, 1H), 7.70 (s, 1H), 7.66−7.61 (m, 3H), 7.46 (t, J = 7.3 Hz, 2H), 7.40−7.36 (m, 3H), 7.26 (d, J = 7.9 Hz, 1H), 7.19 (t, J = 7.6 Hz, 1H), 6.93 (d, J = 15.6 Hz, 1H), 2.28 (s, 3H). ^{13}C

https://doi.org/10.1021/acs.jmedchem.0c02129
J. Med. Chem. 2021, 64, 3976−3996

NMR (101 MHz, DMSO-d_6) δ 167.0, 164.3, 143.4, 141.6, 141.4, 141.1, 135.9, 134.5, 133.9, 131.6, 130.6, 129.3, 128.8, 127.7, 126.4, 123.3, 122.7, 120.9, 117.3, 20.6. HRMS (ESI-TOF$^-$) calcd for $C_{23}H_{18}NO_3$ [M-H]$^-$ m/z 356.1287, found 356.1289.

(E)-2-(3-(2′-Methyl-[1,1′-biphenyl]-4-yl)acrylamido)benzoic Acid (A16). Off-white solid. Yield: 45%. mp 218−219 °C. ^{1}H NMR (400 MHz, DMSO-d_6) δ 11.47 (s, 1H), 8.68 (d, J = 8.3 Hz, 1H), 8.03 (d, J = 7.8 Hz, 1H), 7.75−7.67 (m, 3H), 7.60 (t, J = 7.7 Hz, 1H), 7.36 (d, J = 7.5 Hz, 2H), 7.25−7.14 (m, 5H), 6.90 (d, J = 15.6 Hz, 1H), 2.22 (s, 3H). ^{13}C NMR (101 MHz, DMSO-d_6) δ 170.1, 164.3, 143.4, 141.5, 141.4, 141.0, 135.1, 134.5, 133.5, 131.6, 130.9, 123.0, 129.8, 128.5, 128.0, 126.5, 123.3, 122.8, 120.8, 117.2, 20.6. HRMS (ESI-TOF$^-$) calcd for $C_{23}H_{18}NO_3$ [M-H]$^-$ m/z 356.1287, found 356.1281.

(E)-2-(3-(2′-Methoxy-[1,1′-biphenyl]-4-yl)acrylamido)benzoic Acid (A17). Off-white solid. Yield: 55%. mp 217−219 °C. ^{1}H NMR (400 MHz, DMSO-d_6) δ 13.69 (br s, 1H), 11.39 (s, 1H), 8.65 (d, J = 8.4 Hz, 1H), 8.03 (d, J = 7.9 Hz, 1H), 7.76 (d, J = 7.8 Hz, 2H), 7.70−7.61(m, 2H), 7.55 (d, J = 7.7 Hz, 2H), 7.39−7.33 (m, 2H), 7.19 (t, J = 7.6 Hz, 1H), 7.13 (d, J = 8.2 Hz, 1H), 7.05 (t, J = 7.4 Hz, 1H), 6.91 (d, J = 15.6 Hz, 1H), 3.78 (s, 3H). ^{13}C NMR (101 MHz, DMSO-d_6) δ 170.0, 169.5, 164.3, 156.7, 141.6, 141.4, 140.3, 134.5, 133.4, 131.6, 130.7, 130.2, 129.5, 128.4, 123.3, 122.6, 121.3, 120.9, 117.3, 112.3, 56.0. HRMS (ESI-TOF$^-$) calcd for $C_{23}H_{18}NO_4$ [M-H]$^-$ m/z 372.1236, found 372.1238.

(E)-2-(3-(2′-Fluoro-[1,1′-biphenyl]-4-yl)acrylamido)benzoic Acid (A18). Off-white solid. Yield: 32%. mp 227−228 °C. ^{1}H NMR (400 MHz, DMSO-d_6) δ 13.70 (s, 1H), 11.40 (s, 1H), 8.63 (d, J = 8.3 Hz, 1H), 8.03 (d, J = 7.9 Hz, 1H), 7.86 (d, J = 8.2 Hz, 2H), 7.71−7.57 (m, 5H), 7.48−7.43 (m, 1H), 7.37−7.31 (m, 2H), 7.20 (t, J = 7.6 Hz, 1H), 6.98 (d, J = 15.6 Hz, 1H). ^{13}C NMR (101 MHz, DMSO-d_6) δ 170.0, 164.2, 159.6 (d, J_{CF} = 247.5 Hz), 141.26 (d, J_{CF} = 3.7 Hz), 137.0, 134.5, 134.4, 131.6, 131.2 (d, J_{CF} = 3.1 Hz), 130.5, 130.4, 129.8 (d, J_{CF} = 2.9 Hz), 128.9, 128.1, 128.0, 125.5 (d, J_{CF} = 3.3 Hz), 123.4, 123.3, 120.9, 117.4, 116.8, 116.6. ^{19}F NMR (376 MHz, DMSO-d_6) δ −118.0. HRMS (ESI-TOF$^-$) calcd for $C_{22}H_{15}NO_3F$ [M-H]$^-$ m/z 360.1036, found 360.1035.

(E)-2-(3-(2′-(Trifluoromethyl)-[1,1′-biphenyl]-4-yl)acrylamido)-benzoic Acid (A19). Off-white solid. Yield: 38%. mp 206−208 °C. ^{1}H NMR (400 MHz, DMSO-d_6) δ 13.69 (s, 1H), 11.42 (s, 1H), 8.65 (d, J = 8.2 Hz, 1H), 8.03 (dd, J = 7.9, 1.5 Hz, 1H), 7.86−7.81 (m, 3H), 7.76−7.69 (m, 2H), 7.66−7.61 (m, 2H), 7.44 (d, J = 7.5 Hz, 1H), 7.38 (d, J = 8.1 Hz, 2H), 7.21−7.17 (m, 1H), 6.97 (d, J = 15.6 Hz, 1H). ^{13}C NMR (101 MHz, DMSO-d_6) δ 170.0, 164.2, 141.3, 141., 141.2, 140.5, 140.5, 134.5, 134.4, 132.8, 132.4, 131.6, 129.7, 128.7, 128.3, 127.3 (q, J_{CF} = 30.3 Hz), 126.6 (q, J_{CF} = 6.1 Hz), 124.6 (q, J_{CF} = 274.7 Hz), 123.4, 123.4, 120.9, 117.3. ^{19}F NMR (376 MHz, DMSO-d_6) δ −55.3. HRMS (ESI-TOF$^-$) calcd for $C_{23}H_{15}NO_3F_3$ [M-H]$^-$ m/z 410.1004, found 410.1002.

(E)-2-(3-(3′-Methyl-[1,1′-biphenyl]-4-yl)acrylamido)benzoic Acid (A20). Off-white solid. Yield: 60%. mp 194−196 °C. ^{1}H NMR (400 MHz, DMSO-d_6) δ 13.64 (s, 1H), 11.38 (s, 1H), 8.65 (d, J = 8.4 Hz, 1H), 8.03 (d, J = 7.9 Hz, 1H), 7.81 (d, J = 7.9 Hz, 2H), 7.73−7.61 (m, 4H), 7.53−7.49 (m, 2H), 7.36 (t, J = 7.6 Hz, 1H), 7.21−7.17 (m, 2H), 6.93 (d, J = 15.6 Hz, 1H), 2.38 (s, 3H). ^{13}C NMR (101 MHz, DMSO-d_6) δ 170.0, 164.3, 142.1, 141.4, 139.7, 138.6, 134.5, 134.0, 131.6, 129.4, 129.3, 129.0, 127.8, 127.5, 124.3, 123.3, 122.8, 120.9, 117.3, 27.6. HRMS (ESI-TOF$^-$) calcd for $C_{23}H_{18}NO_3$ [M-H]$^-$ m/z 356.1287, found 356.1284.

(E)-2-(3-(3′-Methoxy-[1,1′-biphenyl]-4-yl)acrylamido)benzoic Acid (A21). Off-white solid. Yield: 52%. mp 259−261 °C. ^{1}H NMR (400 MHz, DMSO-d_6) δ 13.67 (s, 1H), 11.39 (s, 1H), 8.63 (d, J = 8.3 Hz, 1H), 8.02 (dd, J = 7.9, 1.2 Hz, 1H), 7.84 (d, J = 8.3 Hz, 2H), 7.76 (d, J = 8.3 Hz, 2H), 7.70−7.62 (m, 2H), 7.41 (t, J = 7.9 Hz, 1H), 7.31−7.26 (m, 2H), 7.21 (t, J = 7.7 Hz, 1H), 6.99−6.94 (m, 2H), 3.84 (s, 3H). ^{13}C NMR (101 MHz, DMSO-d_6) δ 170.1, 164.2, 160.3, 141.9, 141.5, 141.3,141.2, 134.5, 134.1, 131.7, 130.5, 129.2, 127.6, 123.2, 122.8, 120.8, 119.4, 117.1, 113.8, 112.6, 55.5. HRMS (ESI-TOF$^-$) calcd for $C_{23}H_{18}NO_4$ [M-H]$^-$ m/z 372.1236, found 372.1227.

(E)-2-(3-(3′-Fluoro-[1,1′-biphenyl]-4-yl)acrylamido)benzoic Acid (A22). Off-white solid. Yield: 43%. mp 219−221 °C. ^{1}H NMR (400 MHz, DMSO-d_6) δ 11.43 (s, 1H), 8.66 (d, J = 8.3 Hz, 1H), 8.03 (d, J = 7.7 Hz, 1H), 7.82−7.74 (m, 4H), 7.70−7.60 (m, 2H), 7.56−7.46 (m, 3H), 7.21−7.16 (m, 2H), 6.93 (d, J = 15.6 Hz, 1H). ^{13}C NMR (101 MHz, DMSO-d_6) δ 170.0, 164.2, 163.2 (d, J_{CF} = 244.4 Hz), 142.2 (d, J_{CF} = 7.1 Hz), 141.4, 141.2, 140.4, 134.6, 134.5, 131.6, 131.4, 131.3, 129.3, 127.7, 123.3, 123.1 (d, J_{CF} = 3.0 Hz), 120.8, 117.2, 115.0 (d, J_{CF} = 21.2 Hz), 113.8 (d, J_{CF} = 22.2 Hz). ^{19}F NMR (376 MHz, DMSO-d_6) δ −112.5. HRMS (ESI-TOF$^-$) calcd for $C_{22}H_{15}NO_3F$ [M-H]$^-$ m/z 360.1036, found 360.1034.

(E)-2-(3-(3′-(Trifluoromethyl)-[1,1′-biphenyl]-4-yl)acrylamido)-benzoic Acid (A23). Off-white solid. Yield: 54%. mp 226−228 °C. ^{1}H NMR (400 MHz, DMSO-d_6) δ 13.56 (br s, 1H), 11.39 (s, 1H), 8.64 (d, J = 8.4 Hz, 1H), 8.02 (d, J = 7.9 Hz, 3H), 7.83 (q, J = 7.8 Hz, 4H), 7.86−7.80 (m, 3H), 7.62 (t, J = 7.8 Hz, 1H), 7.18 (t, J = 7.6 Hz, 1H), 6.96 (d, J = 15.6 Hz, 1H). ^{13}C NMR (101 MHz, DMSO-d_6) δ 169.9, 164.2, 141.3, 141.1, 140.8, 140.2, 134.8, 134.4, 131.6, 131.2, 130.5, 130.3 (q, J_{CF} = 31.3 Hz), 129.4, 127.9, 126.0, 124.8, 124.1 (q, J_{CF} = 273.7 Hz), 123.5 (q, J_{CF} = 11.1 Hz), 123.3, 120.9, 117.3. ^{19}F NMR (376 MHz, DMSO-d_6) δ −61.05. HRMS (ESI-TOF$^-$) calcd for $C_{23}H_{15}NO_3F_3$ [M-H]$^-$ m/z 410.1004, found 410.1000.

(E)-2-(3-(4′-Methyl-[1,1′-biphenyl]-4-yl)acrylamido)benzoic Acid (A24). Off-white solid. Yield: 52%. mp 253−255 °C. ^{1}H NMR (400 MHz, DMSO-d_6) δ 13.66 ((br s, 1H), 11.37 (s, 1H), 8.63 (d, J = 8.4 Hz, 1H), 8.03 (d, J = 7.9 Hz, 1H), 7.82 (d, J = 8.0 Hz, 2H), 7.74−7.62 (m, 6H), 7.29 (d, J = 7.8 Hz, 2H), 7.20 (t, J = 7.5 Hz, 1H), 6.93 (d, J = 15.6 Hz, 1H), 2.35 (s, 3H). ^{13}C NMR (101 MHz, DMSO-d_6) δ 169.9, 164.3, 141.9, 141.4, 141.3, 137.8, 136.8, 134.5, 133.7, 131.6, 130.1, 129.3, 127.3, 127.0, 123.4, 122.6, 120.9, 117.3, 21.2. HRMS (ESI-TOF$^-$) calcd for $C_{23}H_{18}NO_3$ [M-H]$^-$ m/z 356.1287, found 356.1271.

(E)-2-(3-(4′-Methoxy-[1,1′-biphenyl]-4-yl)acrylamido)benzoic ac4id (A25). Off-white solid. Yield: 59%. mp 259−261 °C. ^{1}H NMR (400 MHz, DMSO-d_6) δ 13.67 (br s, 1H), 11.46 (s, 1H), 8.63 (d, J = 8.4 Hz, 1H), 8.02 (d, J = 7.8 Hz, 1H), 7.80 (d, J = 8.1 Hz, 2H), 7.72−7.61 (m, 5H), 7.19 (t, J = 7.5 Hz, 1H), 7.05 (d, J = 8.4 Hz, 2H), 6.91 (d, J = 15.7 Hz, 1H), 3.81 (s, 3H). ^{13}C NMR (101 MHz, DMSO-d_6) δ 170.0, 164.3, 159.8, 141.7, 141.4, 141.3, 134.4, 133.3, 132.0, 131.6, 129.3, 128.3, 127.0, 123.3, 122.4, 120.9, 117.5, 115.0, 55.7. HRMS (ESI-TOF$^-$) calcd for $C_{23}H_{18}NO_4$ [M-H]$^-$ m/z 372.1236, found 372.1238.

(E)-2-(3-(4′-Fluoro-[1,1′-biphenyl]-4-yl)acrylamido)benzoic Acid (A26). Off-white solid. Yield: 57%. mp 224−226 °C. ^{1}H NMR (400 MHz, DMSO-d_6) δ 13.65 (s, 1H), 11.37 (s, 1H), 8.63 (d, J = 8.4 Hz, 1H), 8.01 (d, J = 7.9 Hz, 1H), 7.83 (d, J = 7.9 Hz, 2H), 7.77 (t, J = 8.6 Hz, 2H), 7.74−7.62 (m, 4H), 7.31 (t, J = 8.6 Hz, 2H), 7.19 (t, J = 7.5 Hz, 1H), 6.95 (d, J = 15.6 Hz, 1H). ^{13}C NMR (101 MHz, DMSO-d_6) δ 169.9, 164.3, 162.6 (d, J_{CF} = 264.4 Hz), 141.3 (d, J_{CF} = 5.1 Hz), 140.9, 136.2 (d, J_{CF} = 5.1 Hz), 134.5, 134.0, 131.6, 129.3, 129.2 (d, J_{CF} = 10.1 Hz), 127.5, 123.4, 122.9, 120.9, 117.3, 116.4, 116.2. ^{19}F NMR (376 MHz, DMSO-d_6) δ −114.72. HRMS (ESI-TOF$^-$) calcd for $C_{22}H_{15}NO_3F$ [M-H]$^-$ m/z 360.1036, found 360.1026.

(E)-2-(3-(4′-(Trifluoromethyl)-[1,1′-biphenyl]-4-yl)acrylamido)-benzoic Acid (A27). Off-white solid. Yield: 62%. mp 174−176 °C. ^{1}H NMR (400 MHz, DMSO-d_6) δ 13.65 (br s, 1H), 11.39 (s, 1H), 8.64 (d, J = 8.4 Hz, 1H), 8.02 (d, J = 7.9 Hz, 1H), 7.94 (d, J = 8.0 Hz, 2H), 7.87 (d, J = 8.0 Hz, 2H), 7.80 (d, J = 8.0 Hz, 4H), 7.71−7.61 (m, 2H), 7.19 (t, J = 7.6 Hz, 1H), 6.97 (d, J = 15.6 Hz, 1H). ^{13}C NMR (101 MHz, DMSO-d_6) δ 170.0, 164.2, 143.7, 141.3, 141.1, 140.2, 135.0, 134.5, 131.6, 129.4, 128.6 (q, J_{CF} = 31.3 Hz), 128.0, 127.9, 126.3 (q, J_{CF} = 19.8 Hz), 124.8(q, J_{CF} = 292.9 Hz), 123.4, 123.3, 120.9, 117.3. ^{19}F NMR (376 MHz, DMSO-d_6) δ −60.97. HRMS (ESI-TOF$^-$) calcd for $C_{23}H_{15}NO_3F_3$ [M-H]$^-$ m/z 410.1004, found 410.1003.

(E)-2-(3-(3′-Chloro-[1,1′-biphenyl]-4-yl)acrylamido)benzoic Acid (A28). Yellow solid. Yield: 55%. mp 211−213 °C. ^{1}H NMR (400 MHz, DMSO-d_6) δ 13.69 (br s, 1H), 11.44 (s, 1H), 8.64 (d, J = 8.4 Hz, 1H), 8.03 (dd, J = 7.9, 1.4 Hz, 1H), 7.87−7.83 (m, 2H), 7.79−7.75 (m, 3H), 7.72−7.61 (m, 3H), 7.53−7.49 (m, 1H), 7.47−7.44 (m, 1H), 7.19 (t, J = 7.6 Hz, 1H), 6.97 (d, J = 15.6 Hz, 1H). ^{13}C NMR (101 MHz, DMSO-d_6) δ 170.0, 164.2, 141.9, 141.3, 141.1,

https://doi.org/10.1021/acs.jmedchem.0c02129
J. Med. Chem. 2021, 64, 3976−3996

140.3, 134.7, 134.4, 134.3, 131.6, 131.3, 129.4, 128.2, 127.8, 126.9, 125.9, 123.4, 123.3, 120.9, 117. 6. HRMS (ESI-TOF$^-$) calcd for $C_{22}H_{15}NO_3Cl$ [M-H]$^-$ m/z 376.0740, found 376.0735.

(E)-2-(3-(3′-Bromo-[1,1′-biphenyl]-4-yl)acrylamido)benzoic Acid (A29). Off-white solid. Yield: 49%. mp 216−218 °C. ^{1}H NMR (400 MHz, DMSO-d_6) δ 13.69 (s, 1H), 11.40 (s, 1H), 8.62 (d, J = 8.2 Hz, 1H), 8.02 (dd, J = 7.9, 1.3 Hz, 1H), 7.93 (s, 1H), 7.85 (d, J = 8.4 Hz, 2H), 7.79−7.74 (m, 3H), 7.70−7.59 (m, 3H), 7.45 (t, J = 7.9 Hz, 1H), 7.19 (t, J = 7.6 Hz, 1H), 6.98 (d, J = 16.0 Hz, 1H).^{13}C NMR (101 MHz, DMSO-d_6) δ 168.8, 164.3, 142.2, 141.4, 141.1, 140.3, 134.7, 134.4, 131.6, 131.5, 131.1, 129.7, 129.3, 127.7, 126.2, 123.3, 123.2, 123.0, 120.9, 117.4. HRMS (ESI-TOF$^-$) calcd for $C_{22}H_{15}NO_3Br$ [M-H]$^-$ m/z 420.0235, found 420.0238.

(E)-2-(3-(3′-Nitro-[1,1′-biphenyl]-4-yl)acrylamido)benzoic Acid (A30). Off-white solid. Yield: 50%. mp 228−230 °C. ^{1}H NMR (400 MHz, DMSO-d_6) δ 13.67 (br s, 1H), 11.40 (s, 1H), 8.63 (d, J = 8.3 Hz, 1H), 8.47 (s, 1H), 8.23−8.18 (m, 2H), 8.02 (d, J = 7.8 Hz, 1H), 7.88−7.84 (m, 4H), 7.76 (t, J = 8.0 Hz, 1H), 7.68 (d, J = 15.6 Hz, 1H), 7.62 (t, J = 7.3 Hz, 1H), 7.18 (t, J = 7.5 Hz, 1H), 6.96 (d, J = 15.6 Hz, 1H). ^{13}C NMR (101 MHz, DMSO-d_6) δ 170.0, 164.1, 148.9, 141.3, 141.3, 140.9, 139.4, 135.1, 134.4, 133.7, 131.6, 131.0, 129.5, 127.9, 123.6, 123.4, 122.9, 121.5, 120.9, 117.4. HRMS (ESI-TOF$^+$) calcd for $C_{22}H_{17}N_2O_5$ [M-H]$^-$ m/z 389.1137, found 389.1132.

(E)-2-(3-(4′-Ethyl-[1,1′-biphenyl]-4-yl)acrylamido)benzoic Acid (A31). Off-white solid. Yield: 40%. mp 231−233 °C. ^{1}H NMR (400 MHz, DMSO-d_6) δ 13.63 (br s, 1H), 11.36 (s, 1H), 8.63 (d, J = 8.4 Hz, 1H), 8.02 (dd, J = 7.9, 1.5 Hz, 1H), 7.83 (d, J = 8.4 Hz, 2H), 7.74 (d, J = 8.4 Hz, 2H), 7.70−7.62 (m, 4H), 7.33 (d, J = 8.2 Hz, 2H), 7.22−7.18 (m, 1H), 6.94 (d, J = 15.6 Hz, 1H), 2.66 (q, J = 7.5 Hz, 2H), 1.22 (t, J = 7.6 Hz, 3H). ^{13}C NMR (101 MHz, DMSO-d_6) δ 170.0, 164.3, 144.1, 142.0, 141.4, 141.3, 137.1, 134.5, 133.7, 131.6, 129.3, 128.9, 127.3, 127.1, 123.3, 122.7, 120.9, 117.3, 28.3, 16.0. HRMS (ESI-TOF$^-$) calcd for $C_{24}H_{20}NO_3$ [M-H]$^-$ m/z 370.1443, found 370.1449.

(E)-2-(3-(4′-Isopropyl-[1,1′-biphenyl]-4-yl)acrylamido)benzoic Acid (A32). Off-white solid. Yield: 49%. mp 213-215 °C. ^{1}H NMR (400 MHz, DMSO-d_6) δ 13.66 (s, 1H), 11.39 (s, 1H), 8.66 (d, J = 8.3 Hz, 1H), 8.04 (d, J = 7.5 Hz, 1H), 7.81 (d, J = 8.2 Hz, 2H), 7.72−7.62 (m, 6H), 7.33 (d, J = 8.0 Hz, 2H), 7.19 (t, J = 7.5 Hz, 1H), 7.97−7.90 (m, 1H), 2.95−2.89 (m, 1H), 1.22 (d, J = 6.9 Hz, 6H). ^{13}C NMR (101 MHz, DMSO-d_6) δ 170.0, 164.3, 148.7, 142.0, 141.4, 141.4, 137.3, 134.5, 133.7, 131.6, 129.5, 129.3, 127.4, 127.3, 127.1, 123.3, 122.6, 120.9, 117.3, 33.6, 24.3. HRMS (ESI-TOF$^-$) calcd for $C_{25}H_{22}NO_3$ [M-H]$^-$ m/z 384.1600, found 384.1595.

(E)-2-(3-(4′-(tert-Butyl)-[1,1′-biphenyl]-4-yl)acrylamido)benzoic Acid (A33). Off-white solid. Yield: 41%. mp 237−238 °C. ^{1}H NMR (400 MHz, DMSO-d_6) δ 13.67 (br s, 1H), 11.40 (s, 1H), 8.65 (d, J = 8.1 Hz, 1H), 8.03 (d, J = 7.5 Hz, 1H), 7.82−7.64 (m, 8H), 7.48 (d, J = 7.6 Hz, 2H), 7.19 (t, J = 15.5 Hz, 1H), 6.93 (d, J = 15.5 Hz, 1H), 1.31 (s, 9H). ^{13}C NMR (101 MHz, DMSO-d_6) δ 170.0, 164.3, 150.9, 141.9, 141.4, 141.4, 136.9, 134.5, 133.8, 131.6, 129.3, 127.3, 126.8, 126.3, 123.3, 122.6, 120.9, 117.3, 34.7, 31.5. HRMS (ESI-TOF$^-$) calcd for $C_{26}H_{24}NO_3$ [M-H]$^-$ m/z 398.1756, found 398.1749.

(E)-3-(3-(4-Pentylphenyl)acrylamido)benzoic Acid (C1). Off-white solid. Yield: 52%. mp 259−261 °C. ^{1}H NMR (400 MHz, DMSO-d_6) δ 12.99 (s, 1H), 10.37 (s, 1H), 8.32 (s, 1H), 7.95 (d, J = 9.0 Hz, 1H), 7.63−7.54 (m, 4H), 7.46 (t, J = 12.4 Hz, 1H), 7.28 (d, J = 7.6 Hz, 2H), 6.78 (d, J = 15.6 Hz, 1H), 2.61 (t, J = 7.4 Hz, 2H), 1.63−1.55 (m, 2H), 1.34−1.24 (m, 4H), 0.87 (t, J = 6.5 Hz, 3H). ^{13}C NMR (101 MHz, DMSO-d_6) δ 167.6, 164.4, 145.1, 141.0, 140.0, 132.6, 131.8, 129.5, 129,4, 128.3, 124.5, 123.7, 121.5, 120.4, 35.4, 31.3, 30.9, 22.4, 14.4. HRMS (ESI-TOF$^-$) calcd for $C_{21}H_{22}NO_3$ [M-H]$^-$ m/z 336.1600, found 336.1596.

(E)-4-(3-(4-Pentylphenyl)acrylamido)benzoic Acid (C2). Off-white solid. Yield: 46%. mp 284−286 °C. ^{1}H NMR (400 MHz, DMSO-d_6) δ 12.73 (s, 1H), 10.49 (s, 1H), 7.93 (d, J = 8.5 Hz, 2H), 7.83 (d, J = 8.5 Hz, 2H), 7.63−7.53 (m, 3H), 7.26 (d, J = 7.2 Hz, 2H), 6.82 (d, J = 15.7 Hz, 1H), 2.58 (m, 2H), 1.56 (m, 2H), 1.27 (m, 4H), 0.85 (m, 3H). ^{13}C NMR (101 MHz, DMSO-d_6) δ 167.4, 164.5, 145.2, 143.8, 141.4, 132.5, 130.9, 129.4, 128.3, 125.7, 121.3, 118.9, 35.4, 31.3, 30.9, 22.4, 14.4. HRMS (ESI-TOF$^-$) calcd for $C_{21}H_{22}NO_3$ [M-H]$^-$ m/z 336.1600, found 336.1599.

(E)-3-Methyl-2-(3-(4-pentylphenyl)acrylamido)benzoic Acid (C3). Off-white solid. Yield: 49%. mp 126−128 °C. ^{1}H NMR (400 MHz, DMSO-d_6) δ 12.73 (s, 1H), 9.76 (s, 1H), 7.63 (d, J = 6.9 Hz, 1H), 7.56−7.45 (m, 4H), 7.28−7.23 (m, 3H), 6.88 (d, J = 15.8 Hz, 1H), 2.61 (t, J = 16.4 Hz, 2H), 2.24 (s, 3H), 1.63−1.56 (m, 2H), 1.33−1.24 (m, 4H), 0.87 (t, J = 6.9 Hz, 3H). ^{13}C NMR (101 MHz, DMSO-d_6) δ 168.5, 164.3, 144.8, 140.4, 135.8, 135.7, 134.0, 132.7, 129.4, 129.3, 128.2, 128.0, 126.1, 121.5, 35.4, 31.3, 30.9, 22.4, 18.7, 14.4. HRMS (ESI-TOF$^-$) calcd for $C_{22}H_{24}NO_3$ [M-H]$^-$ m/z 350.1756, found 350.1750.

(E)-3,4-Dimethyl-2-(3-(4-pentylphenyl)acrylamido)benzoic Acid (C4). Off-white solid. Yield: 54%. mp 168−170 °C. ^{1}H NMR (400 MHz, DMSO-d_6) δ 12.68 (br s, 1H), 9.77 (s, 1H), 7.58−7.47 (m, 4H), 7.27 (d, J = 7.6 Hz, 2H), 7.17 (d, J = 7.9 Hz, 1H), 6.89 (d, J = 15.7 Hz, 1H), 2.60 (t, J = 7.5 Hz, 2H), 2.32 (s, 3H), 2.10 (s, 3H), 1.62−1.57 (m, 2H), 1.33−1.24 (m, 4H), 0.87 (t, J = 6.6 Hz, 3H). ^{13}C NMR (101 MHz, DMSO-d_6) δ 168.5, 164.5, 144.8, 141.8, 140.2, 136.0, 134.7, 132.8, 129.4, 128.2, 127.7, 127.6, 126.7, 121.7, 35.4, 31.4, 30.9, 22.4, 21.0, 15.0, 14.4. HRMS (ESI-TOF$^-$) calcd for $C_{23}H_{26}NO_3$ [M-H]$^-$ m/z 364.1913, found 364.1911.

(E)-5-Chloro-3-methyl-2-(3-(4-pentylphenyl)acrylamido)benzoic Acid (C5). Off-white solid. Yield: 44%. mp 208−210 °C. ^{1}H NMR (400 MHz, DMSO-d_6) δ 13.06 (s, 1H), 9.79 (s, 1H), 7.59−7.50 (m, 5H), 7.27 (d, J = 7.5 Hz, 2H), 6.87 (d, J = 15.8 Hz, 1H), 2.60 (t, J = 7.4 Hz, 2H), 2.25 (s, 3H), 1.62−1.55 (m, 2H), 1.34−1.29 (m, 4H), 0.87 (t, J = 6.3 Hz, 3H). ^{13}C NMR (101 MHz, DMSO-d_6) δ 167.2, 164.5, 145.0, 140.7, 138.4, 134.7, 133.3, 132.6, 131.2, 130.2, 129.4, 128.2, 127.3, 121.2, 35.4, 31.4, 30.9, 22.4, 18.4, 14.4. HRMS (ESI-TOF$^-$) calcd for $C_{22}H_{23}NO_3Cl$ [M-H]$^-$ m/z 384.1366, found 384.1361.

(E)-3-Chloro-2-(3-(4-pentylphenyl)acrylamido)benzoic Acid (C6). Off-white solid. Yield: 62%. mp 174−176 °C. ^{1}H NMR (400 MHz, DMSO-d_6) δ 13.00 (br s, 1H), 10.01 (s, 1H), 7.73 (d, J = 7.9 Hz, 2H), 7.56−7.51 (m, 3H), 7.37 (t, J = 7.9 Hz, 1H), 7.28 (d, J = 7.9 Hz, 2H), 6.91 (d, J = 15.8 Hz, 1H), 2.61 (t, J = 16.8 Hz, 2H), 1.63−1.55 (m, 2H), 1.33−1.24 (m, 4H), 0.87 (t, J = 6.8 Hz, 3H). ^{13}C NMR (101 MHz, DMSO-d_6) δ 167.4, 164.6, 145.0, 141.0, 134.2, 132.9, 132.6, 132.1, 131.5, 129.4, 129.1, 128.2, 127.5, 121.0, 35.4, 31.4, 30.9, 22.4, 14.4. HRMS (ESI-TOF$^-$) calcd for $C_{21}H_{21}NO_3Cl$ [M-H]$^-$ m/z 370.1210, found 370.1205.

(E)-4-Methyl-2-(3-(4-pentylphenyl)acrylamido)benzoic Acid (C7). Off-white solid. Yield: 63%. mp 190−192 °C. ^{1}H NMR (400 MHz, DMSO-d_6) δ 13.47 (s, 1H), 11.38 (s, 1H), 8.50 (s, 1H), 7.91 (d, J = 8.1 Hz, 1H), 7.64−7.57 (m, 3H), 7.25 (d, J = 8.1 Hz, 2H), 7.00 (dd, J = 8.1, 1.0 Hz, 1H), 6.80 (d, J = 15.6 Hz, 1H), 2.60 (t, J = 17.0 Hz, 2H), 2.37 (s, 3H), 1.61−1.54 (m, 2H), 1.33−1.24 (m, 4H), 0.86 (t, J = 7.0 Hz, 3H). ^{13}C NMR (101 MHz, DMSO-d_6) δ 170.0, 164.3, 145.2, 145.0, 141.7, 141.6, 132.4, 131.6, 129.3, 128.7, 124.0, 121.9, 120.9, 114.2, 35.4, 31.3, 30.9, 22.4, 22.1, 14.4. HRMS (ESI-TOF$^-$) calcd for $C_{22}H_{24}NO_3$ [M-H]$^-$ m/z 350.1756, found 350.1754.

(E)-4-Methyl-2-(3-(3′-nitro-[1,1′-biphenyl]-4-yl)acrylamido)-benzoic Acid (C8). Yellow solid. Yield: 42%. mp 230−232 °C. ^{1}H NMR (400 MHz, DMSO-d_6) δ 11.99 ((br s, 1H), 8.47 (d, J = 23.9 Hz, 2H), 8.22−8.15 (m, 2H), 7.93 (d, J = 8.0 Hz, 1H), 7.82 (s, 4H), 7.75 (t, J = 8.0 Hz, 1H), 7.64 (d, J = 15.6 Hz, 1H), 6.97−6.88 (m, 2H), 2.35 (s, 3H). ^{13}C NMR (101 MHz, DMSO-d_6) δ 170.5, 163.9, 148.9, 144.0, 141.4, 141.3, 140.5, 139.3, 135.1, 133.6, 131.7, 131.0, 129.4, 127.9, 123.9, 122.9, 121.5, 120.6, 22.1. HRMS (ESI-TOF$^-$) calcd for $C_{23}H_{17}N_2O_5$ [M-H]$^-$ m/z 401.1137, found 401.1139.

(E)-4,5-Difluoro-2-(3-(4-pentylphenyl)acrylamido)benzoic Acid (C9). Off-white solid. Yield: 48%. mp 234−236 °C. ^{1}H NMR (400 MHz, DMSO-d_6) δ 14.11 (br s, 1H), 11.38 (s, 1H), 8.70−8.64 (m, 1H), 7.98−7.93 (m, 1H), 7.63−7.59 (m, 3H), 7.24 (d, J = 8.0 Hz, 2H), 6.81 (d, J = 15.6 Hz, 1H), 2.59 (t, J = 7.6 Hz, 2H), 1.60−1.53 (m, 2H), 1.34−1.22 (m, 4H), 0.85 (t, J = 6.9 Hz, 3H). ^{13}C NMR (101 MHz, DMSO-d_6) δ 168.3, 164.6, 152.5 (dd, J_{CF} = 251.5, 13.0 Hz), 145.7, 144.6 (dd, J_{CF} = 244.4, 14.9 Hz), 142.5, 139.1 (dd, J_{CF} = 10.7, 2.0 Hz), 132.2, 129.3, 128.8, 121.2, 120.1 (d, J = 19.9 Hz),

https://doi.org/10.1021/acs.jmedchem.0c02129
J. Med. Chem. 2021, 64, 3976−3996

114.1, 109.5 (d, J = 23.2 Hz), 35.5, 31.3, 30.9, 22.4, 14.3. ^{19}F NMR (376 MHz, DMSO-d_6) δ −128.30 (d, J = 22.6 Hz), −143.63 (d, J = 22.6 Hz). HRMS (ESI-TOF$^-$) calcd for $C_{21}H_{20}NO_3F_2$ [M-H]$^-$ m/z 372.1411, found 372.1410.

(E)-4-Chloro-2-(3-(4-pentylphenyl)acrylamido)benzoic Acid (C10). Off-white solid. Yield: 62%. mp 174−176 °C. ^{1}H NMR (400 MHz, DMSO-d_6) δ 11.44 (s, 1H), 8.75 d, J = 8.6 Hz, 1H), 8.01 (d, J = 8.6 Hz, 1H), 7.64−7.59 (m, 3H), 7.25−7.21 (m, 3H), 6.81 (d, J = 15.6 Hz, 1H), 2.58 (t, J = 7.6 Hz, 2H), 1.60−1.52 (m, 2H), 1.32−1.23 (m, 4H), 0.85 (t, J = 7.0 Hz, 3H). ^{13}C NMR (101 MHz, DMSO-d_6) δ 169.3, 164.7, 145.5, 142.5, 142.4, 139.0, 133.3, 132.2, 129.3, 128.8, 123.1, 121.4, 120.0, 115.6, 35.5, 31.3, 30.9, 22.4, 14.4. HRMS (ESI-TOF$^-$) calcd for $C_{21}H_{21}NO_3Cl$ [M-H]$^-$ m/z 370.1210, found 370.1204.

(E)-2-(3-([1,1′-Biphenyl]-4-yl)acrylamido)-4-chlorobenzoic Acid (C11). Off-white solid. Yield: 65%. mp 258−260 °C. ^{1}H NMR (400 MHz, DMSO-d_6) δ 13.89 (br s, 1H), 11.54 (s, 1H), 8.77 (s, 1H), 8.03 (d, J = 8.8 Hz, 1H), 7.86 (d, J = 12.2 Hz, 2H), 7.77−7.68 (m, 5H), 7.50 (t, J = 13.6 Hz, 2H), 7.40 (t, J = 7.2 Hz, 1H), 7.26 (d, J = 8.6 Hz, 1H), 6.97 (d, J = 10.1 Hz, 1H). ^{13}C NMR (101 MHz, DMSO-d_6) δ 169.2, 164.6, 142.4, 142.2, 141.9, 139.7, 138.7, 133.9, 133.4, 129.5, 129.4, 128.4, 127.6, 127.2, 123.2, 122.5, 120.0, 116.2. HRMS (ESI-TOF$^-$) calcd for $C_{22}H_{15}NO_3Cl$ [M-H]$^-$ m/z 376.0740, found 376.0742.

(E)-5-Methyl-2-(3-(4-pentylphenyl)acrylamido)benzoic Acid (C12). Off-white solid. Yield: 59%. mp 174−176 °C. ^{1}H NMR (400 MHz, DMSO-d_6) δ 13.56 (s, 1H), 11.21 (s, 1H), 8.50 (d, J = 8.5 Hz, 1H), 7.82 (d, J = 1.5 Hz, 1H), 7.64−7.56 (m, 3H), 7.44 (dd, J = 8.6, 1.7 Hz, 1H), 7.25 (d, J = 8.0 Hz, 2H), 6.80 (d, J = 15.6 Hz, 1H), 2.59 (t, J = 16.8 Hz, 2H), 2.32 (s, 3H), 1.61−1.54 (m, 2H), 1.33−1.25 (m, 4H), 0.86 (t, J = 6.9 Hz, 3H). ^{13}C NMR (101 MHz, DMSO-d_6) δ 170.0, 164.2, 145.2, 141.5, 139.0, 135.0, 132.5, 132.4, 131.6, 129.3, 128.6, 121.9, 120.9, 117.2, 35.4, 31.3, 30.9, 22.4, 20.7, 14.4. HRMS (ESI-TOF$^-$) calcd for $C_{22}H_{24}NO_3$ [M-H]$^-$ m/z 350.1756, found 350.1747.

(E)-5-Bromo-2-(3-(4-pentylphenyl)acrylamido)benzoic Acid (C13). Off-white solid. Yield: 53%. mp 214−216 °C. ^{1}H NMR (400 MHz, DMSO-d_6) δ 14.00 (br s, 1H), 11.25 (s, 1H), 8.57 (d, J = 9.0 Hz, 1H), 8.07 (s, 1H), 7.79 (d, J = 9.0 Hz, 1H), 7.63−7.58 (m, 3H), 7.24 (d, J = 7.6 Hz, 2H), 6.81 (d, J = 15.6 Hz, 1H), 2.58 (t, J = 7.4 Hz, 2H), 1.58−1.54 (m, 2H), 1.32−1.27 (m, 4H), 0.85 (t, J = 6.5 Hz, 3H). ^{13}C NMR (101 MHz, DMSO-d_6) δ 168.6, 164.4, 145.4, 142.2, 140.5, 136.9, 133.6, 132.3, 129.3, 128.7, 122.9, 121.5, 119.4, 114.7, 35.5, 31.3, 30.9, 22.4, 14.4. HRMS (ESI-TOF$^-$) calcd for $C_{21}H_{21}NO_3Br$ [M-H]$^-$ m/z 414.0705, found 414.0701.

(E)-2-(3-([1,1′-Biphenyl]-4-yl)acrylamido)-5-fluorobenzoic Acid (C14). Off-white solid. Yield: 61%. mp 251−253 °C. ^{1}H NMR (400 MHz, DMSO-d_6) δ 11.50 (s, 1H), 8.64−8.61 (m, 1H), 7.79 (d, J = 8.2 Hz, 2H), 7.78−7.69 (m, 7H), 7.51−7.45 (m, 3H), 7.38 (t, J = 7.2 Hz, 1H), 6.92 (d, J = 15.6 Hz, 1H). ^{13}C NMR (101 MHz, DMSO-d_6) δ 168.8, 164.1, 157.4 (d, J_{CF} = 242.4 Hz), 141.9, 141.2, 139.7, 137.6 (d, J_{CF} = 2.0 Hz), 134.0, 129.5, 129.3, 128.4, 127.5, 127.1, 123.0 (d, J_{CF} = 7.1 Hz), 122.7, 120.8 (d, J_{CF} = 22.2 Hz), 120.4, 117.4 (d, J_{CF} = 23.2 Hz). ^{19}F NMR (376 MHz, DMSO-d_6) δ −118.9. HRMS (ESI-TOF$^-$) calcd for $C_{22}H_{15}NO_3F$ [M-H]$^-$ m/z 360.1036, found 360.1031.

(E)-2-(3-([1,1′-Biphenyl]-4-yl)acrylamido)-5-chlorobenzoic Acid (C15). Off-white solid. Yield: 57%. mp 260−262 °C. ^{1}H NMR (400 MHz, DMSO-d_6) δ 14.09 (br s, 1H), 11.37 (s, 1H), 8.63 (d, J = 9.0 Hz, 1H), 7.95 (d, J = 2.6 Hz, 1H), 7.83 (d, J = 8.3 Hz, 2H), 7.75−7.66 (m, 6H), 7.49 (t, J = 7.5 Hz, 2H), 7.40 (t, J = 7.3 Hz, 1H), 6.95 (d, J = 15.6 Hz, 1H). ^{13}C NMR (101 MHz, DMSO-d_6) δ 168.8, 164.3, 142.0, 141.6, 140.1, 139.7, 133.9, 130.8, 129.5, 129.3, 128.3, 127.5, 127.1, 126.9, 122.6, 122.5, 119.3. HRMS (ESI-TOF$^-$) calcd for $C_{22}H_{15}NO_3Cl$ [M-H]$^-$ m/z 376.0740, found 376.0741.

(E)-2-(3-([1,1′-Biphenyl]-4-yl)acrylamido)-5-brmobenzoic Acid (C16). Off-white solid. Yield: 57%. mp 270−272 °C. ^{1}H NMR (400 MHz, DMSO-d_6) δ 13.97 (br s, 1H), 11.30 (s, 1H), 8.58 (d, J = 9.1 Hz, 1H), 8.08 (s, 1H), 7.84−7.81 (m, 3H), 7.76−7.67 (m, 5H), 7.50 (t, J = 13.7 Hz, 2H), 7.40 (t, J = 7.2 Hz, 1H), 6.96 (d, J = 10.5 Hz, 1H). ^{13}C NMR (101 MHz, DMSO-d_6) δ 168.6, 164.3, 142.1, 141.7, 140.4, 139.7, 136.9, 134.0, 133.6, 129.5, 129.4, 128.4, 127.6, 127.2, 123.1, 122.5, 119.7, 114.8. HRMS (ESI-TOF$^-$) calcd for $C_{22}H_{15}NO_3Br$ [M-H]$^-$ m/z 420.0235, found 420.0239.

(E)-5-Bromo-2-(3-(3′-nitro-[1,1′-biphenyl]-4-yl)acrylamido)-benzoic Acid (C17). Off-white solid. Yield: 45%. mp 278−280 °C. ^{1}H NMR (400 MHz, DMSO-d_6) δ 13.56 (s, 1H), 9.19 (s, 1H), 8.58 (d, J = 9.0 Hz, 1H), 8.44 (s, 1H), 8.22−8.16 (m, 3H), 7.80−7.73 (m, 5H), 7.64−7.55 (m, 2H), 6.82 (d, J = 15.7, 1H). ^{13}C NMR (101 MHz, DMSO-d_6) δ 169.1, 163.8, 148.9, 141.3, 140.4, 140.1, 139.3, 135.2, 134.1, 134.0, 133.7, 131.0, 129.3, 127.9, 125.4, 124.1, 122.9, 121.6, 121.5, 114.2. HRMS (ESI-TOF$^-$) calcd for $C_{22}H_{14}N_2O_5Br$ [M-H]$^-$ m/z 465.0086, found 465.0083.

The Synthesis of Compound B1. The synthesis of compound **B1** was mainly done according to a literature method.[41]

A mixture of 1-iodo-4-pentylbenzene **17** (493 mg, 1.8 mmol), 2-vinylbenzoic acid **18** (296 mg, 2 mmol), palladium acetate (0.9 mg, 0.004 mmol), and triethylamine (0.3 mL) in 5 mL of acetonitrile was heated to reflux for 12 h. After it cooled, it was diluted with H_2O, and K_2CO_3 powder was added to maintain the pH at 11. The mixture was extracted with Et_2O three times. The water layer was acidified to pH 2 with 1 N HCl and extracted with EtOAc three times, and the combined organic layers were washed with brne, dried over anhydrous Na_2SO_4, filtered, and concentrated. The crude product was purified by silica gel column chromatography eluting with DCM/MeOH (100/3) to afford compound **B1**.

(E)-2-(4-Pentylstyryl)benzoic Acid (B1). Brown solid. Yield: 74%. mp 128−130 °C. ^{1}H NMR (400 MHz, DMSO-d_6) δ 13.04 (s, 1H), 7.92−7.81 (m, 3H), 7.56 (t, J = 7.0 Hz, 1H), 7.46 (d, J = 7.2 Hz, 2H), 7.37 (t, J = 7.0 Hz, 1H), 7.21−7.11 (m, 3H), 2.56 (t, J = 6.8 Hz, 2H), 1.56 (m, 2H), 1.28 (m, 4H), 0.85 (m, 3H). ^{13}C NMR (101 MHz, DMSO-d_6) δ 169.1, 142.8, 138.4, 135.1, 132.3, 131.1, 130.8, 130.1, 129.2, 127.7, 127.1, 127.0, 126.6, 35.4, 31.3, 31.0, 22.4, 14.4. HRMS (ESI-TOF$^-$) calcd for $C_{20}H_{21}O_2$ [M-H]$^-$ m/z 293.1542, found 293.1533.

The Synthesis of Compound B2. An aqueous solution of NaOH (1.5 M, 2 mL) was added to a solution of 4-pentylbenzaldehyde **16n** (352 mg, 2 mmol) and 2-acetylbenzoic acid **19** (328 mg, 2 mmol) in ethanol (EtOH) (2 mL) at 0 °C. After it was stirred at rt for another 20 h, the resultant mixture was poured into icy water and neutralized by 1 N HCl. The crude product as a solid was collected by filtration and recrystallized from EtOAc to give compound **B2**.[42]

(E)-2-(3-(4-Pentylphenyl)acryloyl)benzoic Acid (B2). Off-white solid. Yield: 69%. mp 102−104 °C. ^{1}H NMR (400 MHz, DMSO-d_6) δ 8.11 (d, J = 7.8 Hz, 1H), 7.70−7.66 (m, 1H), 7.60−7.56 (m, 1H), 7.46−7.42 (m, 3H), 7.22−7.19 (m, 3H), 7.05−7.01 (m, 1H), 2.63 (t, J = 16.2 Hz, 2H), 1.66−1.58 (m, 2H), 1.36−1.30 (m, 4H), 0.90 (t, J = 6.8 Hz, 3H). ^{13}C NMR (101 MHz, DMSO-d_6) δ 197.1, 171.2, 146.3, 146.2, 142.7, 133.07, 131.9, 131.1, 129.6, 129.0, 128.6, 128.0, 127.7, 126.6, 35.9, 31.4, 30.9, 22.59, 14.0. HRMS (ESI-TOF$^-$) calcd for $C_{21}H_{21}O_3$ [M-H]$^-$ m/z 321.1491, found 321.1490.

The Synthesis of Compound B3. 4-Pentylbenzoic acid **20** (500 mg, 2.6 mmol) and thionyl chloride (3 mL) were heated together under reflux for 4 h. Any unreacted thionyl chloride was removed under reduced pressure, and the crude product 4-pentylbenzoyl chloride **21** was used without further purification.

A THF solution of 4-pentylbenzoyl chloride **21** (237 mg, 1.3 mmol) was added dropwise to a mixture of 2-aminobenzoic acid **11a** (274 mg, 2 mmol), catalytic amounts of triethylamine, and dry THF (4 mL) in an ice bath, and the mixture was stirred at 0 °C for 15 min, followed by being heated at 60 °C for an additional 3 h. After the solvent was removed under reduced pressure, the residue was extracted with EtOAc three times, and the combined organic layers were washed with brine, dried over anhydrous Na_2SO_4, filtered, and concentrated. The crude product was purified by silica gel column chromatography eluting with DCM/MeOH (100/3) to afford compound **B3**.

2-(4-Pentylbenzamido)benzoic Acid (B3). Off-white solid. Yield: 58%. mp 126−128 °C. ^{1}H NMR (400 MHz, DMSO-d_6) δ 13.77 (s, 1H), 12.16 (s, 1H), 8.73 (d, J = 6.2 Hz, 1H), 8.07 (d, J = 6.1 Hz, 1H),

https://doi.org/10.1021/acs.jmedchem.0c02129
J. Med. Chem. 2021, 64, 3976−3996

7.88 (d, J = 6.4 Hz, 2H), 7.67 (t, J = 16.4 Hz, 1H), 7.42 (d, J = 6.4 Hz, 2H), 7.20 (t, J = 12.6 Hz, 1H), 2.67 (t, J = 9.8, 2H), 1.63−1.60 (m, 2H), 1.35−1.23 (m, 4H), 0.88 (t, J = 11.7, 3H). ^{13}C NMR (101 MHz, DMSO-d_6) δ 170.5, 165.1, 147.6, 141.8, 134.8, 132.4, 131.8, 129.3, 127.5, 123.3, 120.3, 116.8, 35.4, 31.3, 30.8, 22.4, 14.4. HRMS (ESI-TOF$^-$) calcd for $C_{19}H_{20}NO_3$ [M-H]$^-$ m/z 310.1443, found 310.1448.

The Synthesis of Compound B4. 4-Pentylaniline **22** (148 mg, 1 mmol) was added dropwise to a solution of isobenzofuran-1,3-dione **23** (163 mg, 1 mmol) in acetone (3 mL) at 0 °C. After it was stirred at rt for another 2 h, the resulting precipitate was filtered, recrystallized from ethanol, and dried to afford compound **B4**.[43]

2-((4-Pentylphenyl)carbamoyl)benzoic Acid (B4). Off-white solid. Yield: 84%. mp 172−174 °C. ^{1}H NMR (400 MHz, DMSO-d_6) δ 12.89 (s, 1H), 10.24 (s, 1H), 7.88 (d, J = 7.6 Hz, 1H), 7.67−7.53 (m, 5H), 7.14 (d, J = 7.8 Hz, 2H), 2.54 (t, J = 7.6 Hz, 2H), 1.60−1.53 (m, 2H), 1.35−1.27 (m, 4H), 0.88 (t, J = 6.6 Hz, 3H). ^{13}C NMR (101 MHz, DMSO-d_6) δ 168.0, 167.6, 139.4, 137.4, 132.1, 130.5, 129.9, 129.7, 128.8, 128.2, 120.0, 35.1, 31.3, 31.2, 22.4, 14.4. HRMS (ESI-TOF$^-$) calcd for $C_{19}H_{20}NO_3$ [M-H]$^-$ m/z 310.1443, found 310.1442.

The Synthesis of Compound C18. Compound **A13** (172 mg, 0.5 mmol) and acetic anhydride (3 mL) were heated together under reflux for 2 h. The excess of acetic anhydride was removed under reduced pressure. The crude product was recrystallized from ethanol and dried to afford compound **C18**.

(E)-7-(3-([1,1′-Biphenyl]-4-yl)acryloyl)-7-azabicyclo[4.2.0]octa-1,3,5-trien-8-one (C18). Yellow solid. Yield: 57%. mp 172−174 °C. ^{1}H NMR (400 MHz, DMSO-d_6) δ 8.14 (dd, J = 7.8, 1.1 Hz, 1H), 7.96−7.91 (m, 3H), 7.84 (d, J = 16.2 Hz, 1H), 7.76 (t, J = 17.6 Hz, 4H), 7.66−7.59 (m, 2H), 7.50 (t, J = 7.6 Hz, 2H), 7.42 (t, J = 7.3 Hz, 1H), 7.07 (d, J = 16.2 Hz, 1H). ^{13}C NMR (101 MHz, DMSO-d_6) δ 159.3, 157.4, 147.1, 142.3, 141.1, 139.7, 137.3, 134.1, 129.5, 129.4, 128.9, 128.6, 128.4, 127.6, 127.2, 119.7, 117.3, 100.0. HRMS (ESI-TOF$^+$) calcd for $C_{22}H_{16}NO_2$ [M + H]$^+$ m/z 326.1181, found 326.1187.

General Procedure for the Synthesis of Compounds C19−C22. Piperidine (376 mg, 4.4 mmol) was added to a suspension of benzaldehyde derivatives **16m** or **16n** (4.4 mmol) and malonic acid (416 mg, 4 mmol) in toluene (6 mL). The mixture was heated to reflux for 4 h, followed by being stirred at room temperature for an additional 1 h and then acidified with 1 N HCl. The resulting precipitate was filtered and dried to afford cinnamic acids **24a** and **24b**.

Cinnamic acid **24a** or **24b** (2.6 mmol) and thionyl chloride (3 mL) were heated together under reflux for 4 h. Any unreacted thionyl chloride was removed under reduced pressure, and the crude product, cinnamoyl chloride **25a** or **25b**, was used without further purification.

A THF solution of cinnamoyl chloride **25a** or **25b** (1.3 mmol) was added dropwise to a mixture of 2,3-dihydroquinolin-4(1*H*)-one or 1,2,3,4-tetrahydro-5*H*-benzo[*b*]azepin-5-one (2 mmol), catalytic amounts of triethylamine, and dry THF (4 mL) in an ice bath, and the mixture was stirred at 0 °C for 15 min, followed by being heated at 60 °C for an additional 3 h. After the solvent was removed under reduced pressure, the residue was extracted with EtOAc three times, and the combined organic layers were washed with brine, dried over anhydrous Na_2SO_4, filtered, and concentrated. The crude product was purified by silica gel column chromatography eluting with DCM/MeOH (100/3) to afford compounds **C19−C22**.

(E)-1-(3-([1,1′-Biphenyl]-4-yl)acryloyl)-2,3-dihydroquinolin-4(1H)-one (C19). Off-white solid. Yield: 57%. mp 232−234 °C. ^{1}H NMR (400 MHz, DMSO-d_6) δ 7.93 (dd, J = 7.8, 1.4 Hz, 1H), 7.77−7.70 (m, 7H), 7.68−7.64 (m, 1H), 7.52−7.47 (m, 3H), 7.42−7.33 (m, 2H), 7.16 (d, J = 15.5 Hz, 1H), 4.32 (t, J = 6.2 Hz, 2H), 2.83 (t, J = 6.2 Hz, 2H). ^{13}C NMR (101 MHz, DMSO-d_6) δ 194.3, 165.5, 144.2, 142.4, 142.0, 139.7, 134.6, 134.4, 129.5, 129.2, 128.4, 127.6, 127.4, 127.1, 125.8, 125.5, 124.8, 120.2, 55.4, 44.1. HRMS (ESI-TOF$^+$) calcd for $C_{24}H_{20}NO_2$ [M + H]$^+$ m/z 354.1494, found 354.1500.

(E)-1-(3-(4-Pentylphenyl)acryloyl)-2,3-dihydroquinolin-4(1H)-one (C20). Off-white solid. Yield: 46%. mp 78−80 °C. ^{1}H NMR (400 MHz, $CDCl_3$) δ 8.08 (dd, J = 8.0, 1.6 Hz, 1H), 7.82 (d, J = 15.5 Hz, 1H), 7.58−7.53 (m, 1H), 7.42 (d, J = 8.1 Hz, 2H), 7.33−7.28 (m, 2H), 7.20 (d, J = 8.1 Hz, 2H), 6.88 (d, J = 15.5 Hz, 1H), 4.41 (t, J = 6.3 Hz, 2H), 2.87 (t, J = 6.3 Hz, 2H), 2.63 (t, J = 12.2 Hz, 2H), 1.67−1.59 (m, 2H), 1.38−1.30 (m, 4H), 0.91 (t, J = 6.8 Hz, 3H). ^{13}C NMR (101 MHz, $CDCl_3$) δ 194.0, 165.8, 145.7, 143.9, 143.8, 134.0, 132.3, 129.0, 128.1, 128.0, 125.7, 125.4, 124.0, 117.8, 43.6, 39.7, 35.8, 31.4, 30.9, 22.5, 14.0. HRMS (ESI-TOF$^+$) calcd for $C_{23}H_{26}NO_2$ [M + H]$^+$ m/z 348.1964, found 348.1959.

(E)-1-(3-([1,1′-Biphenyl]-4-yl)acryloyl)-3,4-dihydro-1H-benzo[b]-azepin-5(2H)-one (C21). Off-white solid. Yield: 57%. mp 213−215 °C. ^{1}H NMR (400 MHz, $CDCl_3$) δ 8.00 (d, J = 7.7 Hz, 1H), 7.81 (d, J = 15.5 Hz, 1H), 7.64−7.53 (m, 5H), 7.51−7.35 (m, 6H), 7.28−7.27 (m, 1H), 6.42 (d, J = 15.4 Hz, 1H), 4.98 (m, 1H), 3.23 (m, 1H), 2.78 (m, 2H), 2.34 (m, 1H), 1.94 (m, 1H). ^{13}C NMR (101 MHz, $CDCl_3$) δ 201.6, 166.1, 142.6, 141.8, 140.1, 135.0, 133.8, 133.4, 130.0, 128.9, 128.5, 128.1, 127.8, 127.4, 127.0, 118.1, 46.5, 40.1, 22.2. HRMS (ESI-TOF$^+$) calcd for $C_{25}H_{22}NO_2$ [M + H]$^+$ m/z 368.1651, found 368.1642.

(E)-1-(3-(4-Pentylphenyl)acryloyl)-3,4-dihydro-1H-benzo[b]-azepin-5(2H)-one (C22). Yellow oil. Yield: 44%. ^{1}H NMR (400 MHz, DMSO-d_6) δ 7.82 (d, J = 7.6 Hz, 1H), 7.66 (t, J = 10.9 Hz, 1H), 7.59 (d, J = 15.5 Hz, 1H), 7.53−7.51 (m, 1H), 7.34−7.29 (m, 3H), 7.13 (d, J = 7.1 Hz, 2H), 6.33 (d, J = 13.7 Hz, 1H), 2.62 (m, 2H), 2.14−1.80 (m, 2H), 1.53−1.47 (m, 2H), 1.27−1.19 (m, 4H), 0.81 (t, J = 6.9 Hz, 3H). ^{13}C NMR (101 MHz, DMSO-d_6) δ 201.6, 165.6, 145.1, 142.1, 135.0, 133.9, 132.6, 129.5, 129.4, 129.3, 128.3, 118.3, 46.4, 35.4, 31.3, 30.9, 27.7, 22.4, 14.3. HRMS (ESI-TOF$^+$) calcd for $C_{24}H_{28}NO_2$ [M + H]$^+$ m/z 362.2120, found 362.2116.

Cell Culture and Transfection. The tetracycline-inducible HEK293T cells were cultured in DMEM/F-12 (Gibco) plus 10% fetal bovine serum (FBS) with 1 μg/mL tetracycline (Sigma) as previously described.[50,51] SH-SY5Y cells were cultured in DMEM (Gibco) supplemented with 10% FBS. All cells were cultured at 37 °C under a humidified atmosphere containing 5% CO_2. HEK293T cells were used to transiently express wild-type TRPM8 or TRPV1. The 1 μg of human TRPM8 or mouse TRPV1 and 50 ng of green fluorescent protein were together transfected into HEK293T cells using Lipofectamine 2000 (Invitrogen) for 24−48 h before recordings. Cells were seeded on coverslips before use.

Calcium Fluorescent Measurements. Free $[Ca^{2+}]_i$ was determined using Fluo-3/AM (Invitrogen) as previously described.[28] Cells in 96-well plates (3603; Costar) were incubated with 3.5 μM Fluo-3/AM at 37 °C for 0.5 h and washed with Hanks' balanced salt solution, and the fluorescence intensity was measured using a SynergyMx M5 microplate reader (Molecular Devices) with excitation at 485 nm and emission at 525 nm. The intensity of the control well, in which 1 mM H_2O_2 was added, was set as 100%, and the data were normalized as percentages of the control. Each group had three replicate wells, and all procedures were performed in a dark condition.

Electrophysiology. For the inhibitory activity test on the TRPM2 channel, patch-clamp recordings were performed in a whole-cell configuration at room temperature using Axonpatch 700B (Axon Instruments). Similar to our previously reported protocol,[28,32] cells were kept in an extracellular solution (ECS) containing (in mM): 145 NaCl, 5.6 KCl, 2$MgCl_2$, 1.2 $CaCl_2$, 10 4-(2-hydroxyethyl)-1-piperazineethanesulfonic acid (HEPES), pH 7.2. Electrodes had a final resistance of 3−5 MΩ when filled with an intracellular solution (ICS) containing (in mM) 147 NaCl, 1 ethylene glycol tetraacetic acid (EGTA), 1 $MgCl_2$, 24 HEPES, pH 7.3. Patch pipettes were prepared from the Narishige PC-10 puller (Narishige) with borosilicate glass (Sutter Instrument). The adenosine diphosphate ribose (ADPR) concentration was fixed at 500 μM in the ICS. Test compounds were added to the ECS with the indicated concentrations and perfused for at least 60 s after the ADPR-activated TRPM2 current was stabilized. Acidic ECS (pH 5.0) was applied to block TRPM2 currents. A change in ECS was achieved using the RSC-160 system (Biologic Science Instruments) in which the solution changing time was ∼300 ms. The cell was held at 0 mV. Voltage ramps with a 500 ms duration from −100 to 100 mV were applied every 5 s. Data were acquired at 10 kHz and filtered offline at 50 Hz. The mean of the

https://doi.org/10.1021/acs.jmedchem.0c02129
J. Med. Chem. 2021, 64, 3976−3996

first three ramps before the channel activation was used for a leak subtraction of all the current recording. For a specificity evaluation, recordings were conducted on the TRPM8 and TRPV1 currents. The ECS and ICS of TRPM8 and TRPV1 were the same. The ECS contains (in mM) 130 NaCl, 5 KCl, 10 D-glucose, 10 HEPES, 1.2 $MgCl_2$, and 1.5 $CaCl_2$, pH 7.4. The ICS contains (in mM) 115 CsCl, 10 EGTA, 2 $MgCl_2$, 10 HEPES, and 5.7 $CaCl_2$, pH 7.2. The test compounds were added to the ECS with indicated concentrations and perfused for at least 60 s after the TRPM8 or TRPV1 currents were stabilized. Menthol (1 mM) was added in the ECS to activate the TRPM8 channel, and capsaicin (0.01 mM) was added in the ECS to activate the TRPV1 channel. The inhibition ratio (%) was calculated using this formula: [1 − (residual current after test compound treatment − residual current after pH 5 or ECS treatment)/(stable current after agonist treatment − residual current after pH 5 or ECS treatment)] × 100. The IC_{50} values were derived from fitting the concentration−response relationships to the Hill equation.

OGD/R Procedure. An I/R injury was induced in vitro using the OGD/R model as previously described.[52] OGD was conducted when the SH-SY5Y cells were seeded in a 96-well plate at a cell density of ~2×10^4 cells per well for 12 h. The complete culture medium was changed to glucose-free and serum-free DMEM medium and incubated in a modular incubator chamber (Billups-Rothenberg) with 95% N_2 and 5% CO_2. The chamber was kept in an incubator for 8 h at 37 °C to produce OGD and then cultured under normoxic conditions (5% CO_2, 95% air) in normal DMEM for an additional 12 h. The test compounds were added to normal DMEM before the reperfusion phase. The control culture was always maintained in normal DMEM and placed in the incubator under normoxic conditions. Each group had three replicate wells.

Cell Viability Assessment. The cell viability was detected with the CCK-8 cell proliferation assay kit (Beyotime) in a 96-well plate. Then 2×10^4 SH-SY5Y cells per well were seeded and incubated at 37 °C for 12 h. After the indicated drug treatment, the cells were cultured for a further 24 h. Then the culture medium was changed to one containing 10% CCK8, and the cells were incubated at 37 °C for 2 h. For the OGD/R model, the culture medium was changed to one containing 10% CCK8 after the reperfusion phase. The optical density (OD) at 450 nm wavelength was measured with a SynergyMx M5 microplate reader (Molecular Devices). The cellular viability (%) was calculated using this formula: (experimental group OD − blank group OD mean)/(control group OD mean − blank group OD mean) × 100. Each group had three replicate wells.

Colorimetric PLA2 Assay. This method has been published and was used with minor modifications.[53] Briefly, PLA2 (Sigma) was diluted with phosphate-buffered saline to a concentration of 4 μg/L. The enzyme solution (50 μL) was incubated at 37 °C with 5 μL of an appropriate concentration of inhibitor buffer (125 mmol/L Tris). After 30 min, 50 μL of substrate buffer (12.5 mg of soybean phosphatidylcholine purchased from Sigma, 250 mmol Tris, 8 mmol $CaC1_2$, 4 mmol of sodium desoxycholate, and 0.5% Triton X100 in 1 mL of distilled water) was added and incubated for another 60 min. The liberated free fatty acids were quantitated using the free fatty acid content assay kit in a 96-well plate according to the manufacturer's instructions (Solarbio). The OD at 550 nm wavelength was measured with the SynergyMx M5 microplate reader (Molecular Devices). Results are expressed as the percent inhibition compared with the enzyme activity without inhibitor.

Animal and Treatments. C57BL/6 mice were housed under standard conditions with a 12/12 h light/dark cycle and free access to food and water. Eight- to 10-week-old male mice that weighed 22−26 g were used in the study and were randomly assigned to each group. Compound **A23** was dissolved in 5% DMSO with 5% Solutol dissolved in saline for i.v. and i.g. treatments. All animal use procedures were according to the University Policies on the Use and Care of Animals. All of the experiments were performed at room temperature.

PK Studies. C57BL/6 mice (n = 3/group) were dosed with **A23** via the tail vein for i.v. administration (3, 1, and 0.3 mg/kg, 5% DMSO/5% Solutol in saline) or i.g. administration (10, 100 mg/kg, 5% DMSO/5% Solutol in saline). After the doses were given, the time points for the blood sample collection were 0.083, 0.25, 0.5, 1, 2, 4, 6, 8, and 24 h. And after centrifugation, the plasma samples were extracted with acetonitrile and analyzed by high-pressure liquid chromatography/tandem mass spectrometry (LC/MS/MS) with an ethylene bridged hybrid (BEH) C18 column (50 mm × 2.1 mm, 1.7 μm). The compound detection was performed with the mass spectrometer (XEVO TQ-S micro; Waters Corp.). The PK parameters were calculated with WinNonlin software 8.0 (Pharsight Corporation).

tMCAO Model. As we described in our previous studies,[54,55] we used laser Doppler to monitor the cerebral blood flow (CBF) of each model mouse. Animals with less than an 80% reduction in CBF were excluded from the study. The tMCAO model is stably reproducible in our lab. Briefly, the mice were anesthetized with isoflurane (5% induction, 1.5−2% maintenance) in a 30% oxygen/70% nitrous oxide mix. The right common carotid artery (CCA), internal carotid artery (ICA), and external carotid artery (ECA) were exposed through a midline incision of the neck. A 6−0 nylon monofilament suture, blunted at the tip and coated with 1% poly L-lysine, was inserted from the ECA into the ICA to occlude the origin of the middle cerebral artery (MCA). After 90 min of the occlusion, the nylon suture was removed for reperfusion. After the operation, mice were transferred into an intensive-care chamber with the maintained temperature at 37 °C, until animals woke up completely. The body temperature was maintained at 37.0 ± 0.5 °C throughout the operation and recovery. The number of animals excluded from the hemorrhage is less than 10%.

Experimental Groups and Drug Administration. Mice were randomly divided into four groups as follows: control group (saline), vehicle group (5% DMSO/5% Solutol in saline), **A23** group (0.3, 1, and 3 mg/kg), and EDA group (0.3, 1, and 3 mg/kg). The drugs were administered by i.v. infusion (tail vein) at 3 h after the onset of reperfusion. The control group, vehicle group, **A23** group, and EDA group were injected with the same volume of saline.

Evaluation of Neurological Scores. Neurological scores were evaluated after 24 h of reperfusion by the examiner who was blinded to the treatment conditions to assess the health of mouse.[56] The scores were assigned using the following scale: 0, no neurological deficits; 1, failure to fully extend the right forepaw; 2, circling to the right; 3, falling to the right; and 4, absence of spontaneous walking and depressed levels of consciousness.

Infarct Volume Analysis. After an evaluation of neurological scores, the mice were sacrificed with 10% chloral hydrate injected. Brain tissues were dissected and stored at −20 °C for 20 min. The mice were excluded from the study if a subarachnoid hemorrhage was observed. Then, the brain tissue was removed into the brain slicer matrix and sliced into five 1.0 mm thick coronal sections. The brain slices were incubated for 30 min at 37 °C in 2% TTC solution and were then immersed in 4% paraformaldehyde overnight. The infarct volume was measured by a researcher blinded to the experimental groups using ImageJ software (National Institutes of Health).

Data Analysis. Data are expressed as the mean ± standard deviation (SD) from at least three independent experiments. A statistical analysis was performed using one-way analysis of variance (ANOVA), followed by Dunnett's test or Tukey's test for multiple comparisons, with $P < 0.05$ considered statistically significant. GraphPad Prism 7 software (GraphPad) was used for all statistical analyses.

■ ASSOCIATED CONTENT

Supporting Information

The Supporting Information is available free of charge at https://pubs.acs.org/doi/10.1021/acs.jmedchem.0c02129.

Molecular formula strings of tested compounds (CSV)

Structural formulas of all synthesized final compounds; inhibition activity of selected compounds; cell viability for **A22**, **A23**, **A30**, **C7**, **C12**, and **C16** on SH-SY5Y

https://doi.org/10.1021/acs.jmedchem.0c02129
J. Med. Chem. 2021, 64, 3976−3996

cells; pharmacokinetic parameters of **A23**; ^{1}H NMR, ^{13}C NMR, HRMS, and HPLC data for all synthesized final compounds (PDF)

AUTHOR INFORMATION

Corresponding Authors

Wei Yang − *Department of Biophysics, and Department of Neurosurgery of the First Affiliated Hospital, Zhejiang University School of Medicine, Hangzhou 310058, P. R. China*; Email: yangwei@zju.edu.cn

Liangren Zhang − *State Key Laboratory of Natural and Biomimetic Drugs, School of Pharmaceutical Sciences, Peking University, Beijing 100191, P. R. China*; orcid.org/0000-0002-7362-9497; Email: liangren@bjmu.edu.cn

Authors

Han Zhang − *State Key Laboratory of Natural and Biomimetic Drugs, School of Pharmaceutical Sciences, Peking University, Beijing 100191, P. R. China*

Peilin Yu − *Department of Toxicology, and Department of Medical Oncology of Second Affiliated Hospital, Zhejiang University School of Medicine, Hangzhou 310058, Zhejiang, P. R. China*

Hongwei Lin − *Department of Biophysics, and Department of Neurosurgery of the First Affiliated Hospital, Zhejiang University School of Medicine, Hangzhou 310058, P. R. China*

Zefang Jin − *State Key Laboratory of Natural and Biomimetic Drugs, School of Pharmaceutical Sciences, Peking University, Beijing 100191, P. R. China*

Siqi Zhao − *State Key Laboratory of Natural and Biomimetic Drugs, School of Pharmaceutical Sciences, Peking University, Beijing 100191, P. R. China*

Yi Zhang − *Department of Biophysics, and Department of Neurosurgery of the First Affiliated Hospital, Zhejiang University School of Medicine, Hangzhou 310058, P. R. China*

Qingxia Xu − *State Key Laboratory of Natural and Biomimetic Drugs, School of Pharmaceutical Sciences, Peking University, Beijing 100191, P. R. China*

Hongwei Jin − *State Key Laboratory of Natural and Biomimetic Drugs, School of Pharmaceutical Sciences, Peking University, Beijing 100191, P. R. China*

Zhenming Liu − *State Key Laboratory of Natural and Biomimetic Drugs, School of Pharmaceutical Sciences, Peking University, Beijing 100191, P. R. China*; orcid.org/0000-0002-8993-4015

Complete contact information is available at: https://pubs.acs.org/10.1021/acs.jmedchem.0c02129

Author Contributions

#H.Z. and P.Y. contributed equally to this work.

Notes

The authors declare no competing financial interest.

ACKNOWLEDGMENTS

This research work was financially supported by Key Programs of National Natural Science Foundation of China (82030108 to W.Y. and L.Z.), National Natural Science Foundation of China (81673279 to L.Z. and 32071102 to P.Y.), National Major Special Project on New Drug Innovation of China (2018ZX09711001-004-005 to W.Y.), Beijing Natural Science Foundation (7212152 to L.Z.), Key R & D Projects of Zhejiang Province (2021C03039 to P.Y.), and the Key Research and Development Program of Ningxia Hui Autonomous Region (2019BFH02003 to W.Y.).

ABBREVIATIONS USED

AA, arachidonic acid; ACA, *N*-(*p*-amylcinnamoyl) anthranilic acid; 2-APB, 2-aminoethoxydiphenyl borate; AUC, area under the curve; CCK-8, cell counting kit-8; CL, clearance rate; C_{max}, maximum concentrations; EDA, edaravone; F%, oral bioavailability; FFA, flufenamic acid; HEK293T, human embryonic kidney 293 T cells; I/R, ischemia/reperfusion; i.g., intragastric; i.v., intravenous; 3-MFA, 2-(3-methylphenyl) aminobenzoic acid; MRT, mean residence time; OGD/R, oxygen glucose deprivation/reperfusion; PK, pharmacokinetic; PLA2, phospholipase A2; ROS, reactive oxygen species; SAR, structure−activity relationship; T_{max}, time-to-maximum-concentration; $T_{1/2}$, half-life; tMCAO, transient middle cerebral artery occlusion; TRPM2, transient receptor potential melastatin 2; TRPV1, transient receptor potential vanilloid 1.

REFERENCES

(1) Nilius, B.; Owsianik, G. The transient receptor potential family of ion channels. *Genome Biol.* **2011**, *12*, 218.

(2) Kaneko, Y.; Szallasi, A. Transient receptor potential (TRP) channels: a clinical perspective. *Br. J. Pharmacol.* **2014**, *171*, 2474−2507.

(3) Gees, M.; Owsianik, G.; Nilius, B.; Voets, T. TRP channels. *Compr Physiol.* **2012**, *2*, 563−608.

(4) Pedersen, S. F.; Owsianik, G.; Nilius, B. TRP channels: an overview. *Cell Calcium* **2005**, *38*, 233−252.

(5) Sumoza-Toledo, A.; Penner, R. TRPM2: a multifunctional ion channel for calcium signalling. *J. Physiol.* **2011**, *589*, 1515−1525.

(6) Fonfria, E.; Murdock, P. R.; Cusdin, F. S.; Benham, C. D.; Kelsell, R. E.; McNulty, S. Tissue distribution profiles of the human TRPM cation channel family. *J. Recept. Signal Transduction Res.* **2006**, *26*, 159−178.

(7) Jiang, L. H.; Yang, W.; Zou, J.; Beech, D. J. TRPM2 channel properties, functions and therapeutic potentials. *Expert Opin. Ther. Targets* **2010**, *14*, 973−988.

(8) Tan, C. H.; McNaughton, P. A. TRPM2 and warmth sensation. *Pfluegers Arch.* **2018**, *470*, 787−798.

(9) Gelderblom, M.; Melzer, N.; Schattling, B.; Göb, E.; Hicking, G.; Arunachalam, P.; Bittner, S.; Ufer, F.; Herrmann, A. M.; Bernreuther, C.; Glatzel, M.; Gerloff, C.; Kleinschnitz, C.; Meuth, S. G.; Friese, M. A.; Magnus, T. Transient receptor potential melastatin subfamily member 2 cation channel regulates detrimental immune cell invasion in ischemic stroke. *Stroke* **2014**, *45*, 3395−3402.

(10) Ostapchenko, V. G.; Chen, M.; Guzman, M. S.; Xie, Y. F.; Lavine, N.; Fan, J.; Beraldo, F. H.; Martyn, A. C.; Belrose, J. C.; Mori, Y.; MacDonald, J. F.; Prado, V. F.; Prado, M. A.; Jackson, M. F. The transient receptor potential melastatin 2 (TRPM2) channel contributes to *β*-Amyloid oligomer-related neurotoxicity and memory impairment. *J. Neurosci.* **2015**, *35*, 15157−15169.

(11) Dias, V.; Junn, E.; Mouradian, M. M. The role of oxidative stress in Parkinson's disease. *J. Parkinson's Dis.* **2013**, *3*, 461−491.

(12) Malko, P.; Jiang, L.-H. TRPM2 channel-mediated cell death: an important mechanism linking oxidative stress-inducing pathological factors to associated pathological conditions. *Redox Biol.* **2020**, *37*, 101755.

(13) Miller, B. A. TRPM2 in Cancer. *Cell Calcium* **2019**, *80*, 8−17.

(14) Mozaffarian, D.; Benjamin, E. J.; Go, A. S.; Arnett, D. K.; Blaha, M. J.; Cushman, M.; de Ferranti, S.; Després, J. P.; Fullerton, H. J.; Howard, V. J.; Huffman, M. D.; Judd, S. E.; Kissela, B. M.; Lackland, D. T.; Lichtman, J. H.; Lisabeth, L. D.; Liu, S.; Mackey, R. H.; Matchar, D. B.; McGuire, D. K.; Mohler, E. R., 3rd; Moy, C. S.; Muntner, P.; Mussolino, M. E.; Nasir, K.; Neumar, R. W.; Nichol, G.;

Palaniappan, L.; Pandey, D. K.; Reeves, M. J.; Rodriguez, C. J.; Sorlie, P. D.; Stein, J.; Towfighi, A.; Turan, T. N.; Virani, S. S.; Willey, J. Z.; Woo, D.; Yeh, R. W.; Turner, M. B. Heart disease and stroke statistics–2015 update: a report from the American Heart Association. *Circulation.* **2015**, *131*, e29−322.
(15) Rodrigo, R.; Fernández-Gajardo, R.; Gutiérrez, R.; Matamala, J. M.; Carrasco, R.; Miranda-Merchak, A.; Feuerhake, W. Oxidative stress and pathophysiology of ischemic stroke: novel therapeutic opportunities. *CNS Neurol. Disord.: Drug Targets* **2013**, *12*, 698−714.
(16) Zuo, L.; Feng, Q.; Han, Y.; Chen, M.; Guo, M.; Liu, Z.; Cheng, Y.; Li, G. Therapeutic effect on experimental acute cerebral infarction is enhanced after nanoceria labeling of human umbilical cord mesenchymal stem cells. *Ther Adv. Neurol Disord.* **2019**, *12*, 1−18.
(17) Sanderson, T. H.; Reynolds, C. A.; Kumar, R.; Przyklenk, K.; Hüttemann, M. Molecular mechanisms of ischemia-reperfusion injury in brain: pivotal role of the mitochondrial membrane potential in reactive oxygen species generation. *Mol. Neurobiol.* **2013**, *47*, 9−23.
(18) Zhang, E.; Liao, P. Brain transient receptor potential channels and stroke. *J. Neurosci. Res.* **2015**, *93*, 1165−1183.
(19) Zhan, K. Y.; Yu, P. L.; Liu, C. H.; Luo, J. H.; Yang, W. Detrimental or beneficial: the role of TRPM2 in ischemia/reperfusion injury. *Acta Pharmacol. Sin.* **2016**, *37*, 4−12.
(20) Belrose, J. C.; Jackson, M. F. TRPM2: a candidate therapeutic target for treating neurological diseases. *Acta Pharmacol. Sin.* **2018**, *39*, 722−732.
(21) Zhang, H.; Zhao, S.; Yu, J.; Yang, W.; Liu, Z.; Zhang, L. Medicinal chemistry perspective of TRPM2 channel inhibitors: where we are and where we might be heading? *Drug Discovery Today* **2020**, *25*, 2326−2334.
(22) Hill, K.; Benham, C. D.; McNulty, S.; Randall, A. D. Flufenamic acid is a pH-dependent antagonist of TRPM2 channels. *Neuropharmacology* **2004**, *47*, 450−460.
(23) Hill, K.; McNulty, S.; Randall, A. D. Inhibition of TRPM2 channels by the antifungal agents clotrimazole and econazole. *Naunyn-Schmiedeberg's Arch. Pharmacol.* **2004**, *370*, 227−237.
(24) Kraft, R.; Grimm, C.; Frenzel, H.; Harteneck, C. Inhibition of TRPM2 cation channels by *N*-(p-amylcinnamoyl)anthranilic acid. *Br. J. Pharmacol.* **2006**, *148*, 264−273.
(25) Chen, G. L.; Zeng, B.; Eastmond, S.; Elsenussi, S. E.; Boa, A. N.; Xu, S. Z. Pharmacological comparison of novel synthetic fenamate analogues with econazole and 2-APB on the inhibition of TRPM2 channels. *Br. J. Pharmacol.* **2012**, *167*, 1232−1243.
(26) Nilius, B.; Szallasi, A. Transient receptor potential channels as drug targets: from the science of basic research to the art of medicine. *Pharmacol. Rev.* **2014**, *66*, 676−814.
(27) Starkus, J. G.; Poerzgen, P.; Layugan, K.; Kawabata, K. G.; Goto, J. I.; Suzuki, S.; Myers, G.; Kelly, M.; Penner, R.; Fleig, A.; Horgen, F. D. Scalaradial is a potent inhibitor of transient receptor potential melastatin 2 (TRPM2) ion channels. *J. Nat. Prod.* **2017**, *80*, 2741−2750.
(28) Zhang, H.; Liu, H.; Luo, X.; Wang, Y.; Liu, Y.; Jin, H.; Liu, Z.; Yang, W.; Yu, P.; Zhang, L.; Zhang, L. Design, synthesis and biological activities of 2,3-dihydroquinazolin-4(1*H*)-one derivatives as TRPM2 inhibitors. *Eur. J. Med. Chem.* **2018**, *152*, 235−252.
(29) Fourgeaud, L.; Dvorak, C.; Faouzi, M.; Starkus, J.; Sahdeo, S.; Wang, Q.; Lord, B.; Coate, H.; Taylor, N.; He, Y.; Qin, N.; Wickenden, A.; Carruthers, N.; Lovenberg, T. W.; Penner, R.; Bhattacharya, A. Pharmacology of JNJ-28583113: a novel TRPM2 antagonist. *Eur. J. Pharmacol.* **2019**, *853*, 299−307.
(30) Cruz-Torres, I.; Backos, D. S.; Herson, P. S. Characterization and optimization of the novel transient receptor potential melastatin 2 antagonist tatM2NX. *Mol. Pharmacol.* **2020**, *97*, 102−111.
(31) Moreau, C.; Kirchberger, T.; Swarbrick, J. M.; Bartlett, S. J.; Fliegert, R.; Yorgan, T.; Bauche, A.; Harneit, A.; Guse, A. H.; Potter, B. V. Structure-activity relationship of adenosine 5′-diphosphoribose at the transient receptor potential melastatin 2 (TRPM2) channel: rational design of antagonists. *J. Med. Chem.* **2013**, *56*, 10079−10102.
(32) Luo, X.; Li, M.; Zhan, K.; Yang, W.; Zhang, L.; Wang, K.; Yu, P.; Zhang, L. Selective inhibition of TRPM2 channel by two novel synthesized ADPR analogues. *Chem. Biol. Drug Des.* **2018**, *91*, 552−566.
(33) Jia, J.; Verma, S.; Nakayama, S.; Quillinan, N.; Grafe, M. R.; Hurn, P. D.; Herson, P. S. Sex differences in neuroprotection provided by inhibition of TRPM2 channels following experimental stroke. *J. Cereb. Blood Flow Metab.* **2011**, *31*, 2160−2168.
(34) Verma, S.; Quillinan, N.; Yang, Y. F.; Nakayama, S.; Cheng, J.; Kelley, M. H.; Herson, P. S. TRPM2 channel activation following in vitro ischemia contributes to male hippocampal cell death. *Neurosci. Lett.* **2012**, *530*, 41−46.
(35) Cakir, M.; Duzova, H.; Tekin, S.; Taslıdere, E.; Kaya, G. B.; Cigremis, Y.; Ozgocer, T.; Yologlu, S. ACA, an inhibitor phospholipases A2 and transient receptor potential melastatin-2 channels, attenuates okadaic acid induced neurodegeneration in rats. *Life Sci.* **2017**, *176*, 10−20.
(36) Gao, M.; Du, Y.; Xie, J. W.; Xue, J.; Wang, Y. T.; Qin, L.; Ma, M. M.; Tang, Y. B.; Li, X. Y. Redox signal-mediated TRPM2 promotes Ang II-induced adipocyte insulin resistance via Ca^{2+}-dependent CaMKII/JNK cascade. *Metab., Clin. Exp.* **2018**, *85*, 313−324.
(37) Konrad, R. J.; Jolly, Y. C.; Major, C.; Wolf, B. A. Inhibition of phospholipase A2 and insulin secretion in pancreatic islets. *Biochim. Biophys. Acta, Mol. Cell Res.* **1992**, *1135*, 215−220.
(38) Olsen, H. L.; Nørby, P. L.; Høy, M.; Spee, P.; Thams, P.; Capito, K.; Petersen, J. S.; Gromada, J. Imidazoline NNC77−0074 stimulates Ca^{2+}-evoked exocytosis in INS-1E cells by a phospholipase A2-dependent mechanism. *Biochem. Biophys. Res. Commun.* **2003**, *303*, 1148−1151.
(39) Harteneck, C.; Frenzel, H.; Kraft, R. N-(p-Amylcinnamoyl)-anthranilic acid (ACA): a phospholipase A2 inhibitor and TRP channel blocker. *Cardiovasc. Drug Rev.* **2007**, *25*, 61−75.
(40) Zammit, S. C.; Cox, A. J.; Gow, R. M.; Zhang, Y.; Gilbert, R. E.; Krum, H.; Kelly, D. J.; Williams, S. J. Evaluation and optimization of antifibrotic activity of cinnamoyl anthranilates. *Bioorg. Med. Chem. Lett.* **2009**, *19*, 7003−7006.
(41) Kim, B. M.; Park, J. K. A short synthesis of a chiral alcohol as a new chiral auxiliary for asymmetric reactions. *Bull. Korean Chem. Soc.* **1999**, *20*, 744−746.
(42) Wang, S.; Cao, L.; Shi, H.; Dong, Y.; Sun, J.; Hu, Y. Preparation of 2-pyridone-containing tricyclic alkaloid derivatives as potential inhibitors of tumor cell proliferation by regioselective intramolecular N- and C-acylation of 2-pyridone. *Chem. Pharm. Bull.* **2005**, *53*, 67−71.
(43) Al-Azzawi, A.; Al-Razzak, M. Synthesis, characterization and antibacterial screening of new Schiff bases linked to phthalimide. *Int. J. Res. Pharm. Chem.* **2013**, *3*, 682−690.
(44) Arai, Y.; Toda, M.; Miyamoto, T. Carboxamide derivative, its production and remedy containing said derivative. JP 60097946, 1985.
(45) Yedgar, S.; Cohen, Y.; Shoseyov, D. Control of phospholipase A2 activities for the treatment of inflammatory conditions. *BBA-Mol. Cell Biol. L.* **2006**, *1761*, 1373−1382.
(46) Schiefer, I. T.; VandeVrede, L.; Fa', M.; Arancio, O.; Thatcher, G. R. J. Furoxans (1,2,5-oxadiazole-N-oxides) as novel NO mimetic neuroprotective and procognitive agents. *J. Med. Chem.* **2012**, *55*, 3076−3087.
(47) Song, Y.; Li, M.; Li, J. C.; Wei, E. Q. Edaravone protects PC12 cells from ischemic-like injury via attenuating the damage to mitochondria. *J. Zhejiang Univ., Sci., B* **2006**, *7*, 749−756.
(48) Song, Y.; Bei, Y.; Xiao, Y.; Tong, H. D.; Wu, X. Q.; Chen, M. T. Edaravone, a free radical scavenger, protects neuronal cells' mitochondria from ischemia by inactivating another new critical factor of the 5-lipoxygenase pathway affecting the arachidonic acid metabolism. *Brain Res.* **2018**, *1690*, 96−104.
(49) Davis, C. K.; G K, R. Postischemic supplementation of folic acid improves neuronal survival and regeneration in vitro. *Nutr. Res. (N. Y., NY, U. S.)* **2020**, *75*, 1−14.
(50) Yang, W.; Zou, J.; Xia, R.; Vaal, M. L.; Seymour, V. A.; Luo, J.; Beech, D. J.; Jiang, L. H. State-dependent inhibition of TRPM2 channel by acidic pH. *J. Biol. Chem.* **2010**, *285*, 30411−30418.

https://doi.org/10.1021/acs.jmedchem.0c02129
J. Med. Chem. 2021, 64, 3976−3996

(51) Yang, W.; Manna, P. T.; Zou, J.; Luo, J.; Beech, D. J.; Sivaprasadarao, A.; Jiang, L. H. Zinc inactivates melastatin transient receptor potential 2 channels via the outer pore. *J. Biol. Chem.* **2011**, *286*, 23789−23798.
(52) Wang, H. F.; Wang, Z. Q.; Ding, Y.; Piao, M. H.; Feng, C. S.; Chi, G. F.; Luo, Y. N.; Ge, P. F. Endoplasmic reticulum stress regulates oxygen-glucose deprivation-induced parthanatos in human SH-SY5Y cells via improvement of intracellular ROS. *CNS Neurosci. Ther.* **2018**, *24*, 29−38.
(53) Scheuer, W. Phospholipase A2-regulation and inhibition. *Klin. Wochenschr.* **1989**, *67*, 153−159.
(54) Zhang, B.; Zhang, H. X.; Shi, S. T.; Bai, Y. L.; Zhe, X.; Zhang, S. J.; Li, Y. J. Interleukin-11 treatment protected against cerebral ischemia/reperfusion injury. *Biomed. Pharmacother.* **2019**, *115*, 108816.
(55) Ye, M.; Yang, W.; Ainscough, J. F.; Hu, X. P.; Li, X.; Sedo, A.; Zhang, X. H.; Zhang, X.; Chen, Z.; Li, X. M.; Beech, D. J.; Sivaprasadarao, A.; Luo, J. H.; Jiang, L. H. TRPM2 channel deficiency prevents delayed cytosolic Zn^{2+} accumulation and CA1 pyramidal neuronal death after transient global ischemia. *Cell Death Dis.* **2014**, *5*, No. e1541.
(56) Longa, E. Z.; Weinstein, P. R.; Carlson, S.; Cummins, R. Reversible middle cerebral artery occlusion without craniectomy in rats. *Stroke* **1989**, *20*, 84−91.

https://doi.org/10.1021/acs.jmedchem.0c02129
J. Med. Chem. 2021, 64, 3976−3996